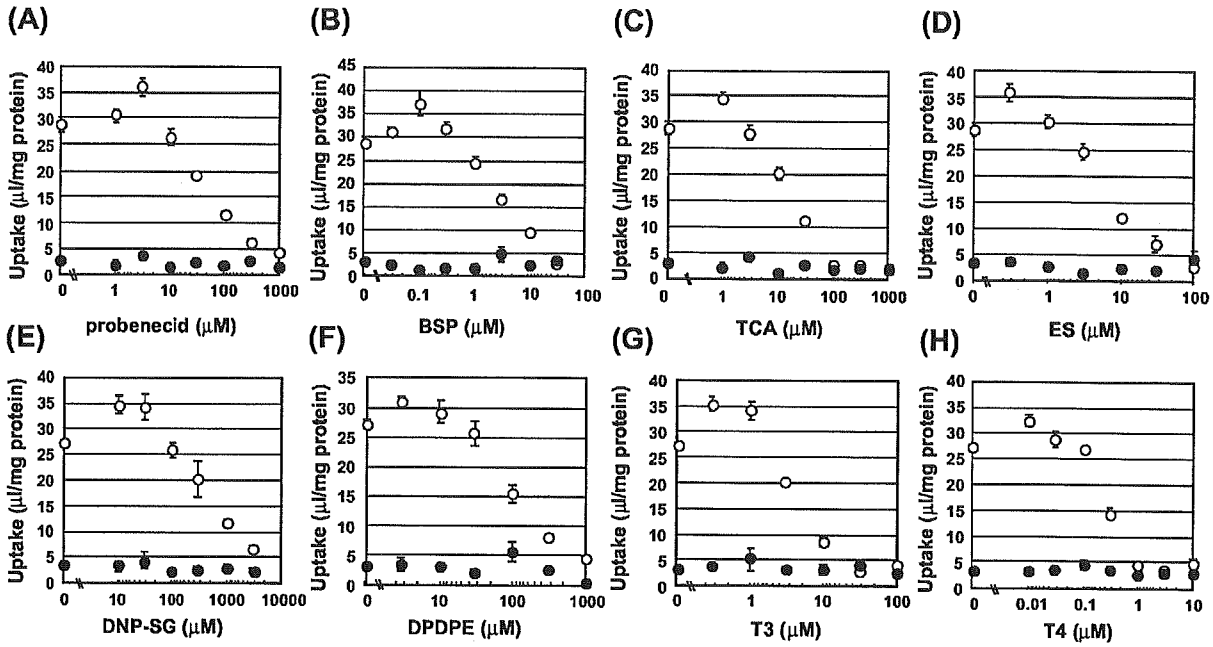

FIG. 5. **Effects of unlabeled probenecid, BSP, trichloroacetic acid, ES, DNP-SG, DPDPE, T_3, and T_4 on the uptake of [^{3}H]$E_2$17βG by Oatp14-transfected HEK293 cells.** The effects of unlabeled probenecid (*A*), BSP (*B*), taurocholate (*TCA*; *C*), ES (*D*), DNP-SG (*E*), DPDPE (*F*), T_3 (*G*), and T_4 (*H*) on the uptake of [^{3}H]$E_2$17βG by Oatp14-transfected HEK293 cells were examined at 37 °C. The specific uptake was obtained by subtracting the uptake by vector-transfected cells from that by gene-transfected cells. *Open* and *closed circles* represent the uptake by Oatp14- and vector-transfected cells, respectively. Each *point* represents the mean ± S.E. (n = 3).

fected cells, and the elimination rate constants were 0.032 ± 0.002 and 0.006 ± 0.001 min^{-1}, respectively (Fig. 4).

cis-inhibitory effects on the Oatp14-mediated uptake of [^{3}H]$E_2$17βG were investigated (Fig. 5). Sulfobromophthalein (BSP), pravastatin, ES, and trichloroacetic acid were potent inhibitors of Oatp14, whereas probenecid was a moderate inhibitor (Fig. 5). *p*-Aminohippurate and cimetidine, typical substrates of organic anion and cation transporters, had no effect on the Oatp14-mediated uptake, whereas benzylpenicillin was a weak inhibitor (Fig. 6). Leukotriene C_4 (*LTC_4*) and glutathione (*GSH*) had no effect, but dinitrophenyl-s-glutathione (*DNP-SG*) was a weak inhibitor (see Figs. 5 and 6). No inhibitory effect by folates (methotrexate, folate, and 5-methyltetrahydrofolate) or tetraethylammonium was observed (Fig. 6). The K_i values of probenecid, BSP, trichloroacetic acid, ES, DNP-SG, DPDPE, T_3, and T_4 for the uptake of [^{3}H]$E_2$17βG by Oatp14-expressed HEK cells are summarized in Table III.

Effects of Hyperthyroid and Hypothyroid Conditions on the Expression of Oatp14 in the Brain Capillary—The effects of hyper- and hypothyroid conditions on the expression of Oatp14 in the brain capillary were investigated by RT-PCR and Western blotting (Fig. 7, *A* and *B*). RT-PCR and Western blotting analyses revealed that the expression levels of Oatp14 mRNA and protein were up- and down-regulated under hypothyroid and hyperthyroid conditions, respectively.

DISCUSSION

In the present study, we reported the substrate specificity of Oatp14, as well as its tissue distribution and localization in the brain. Oatp14 is expressed in the brain capillary and choroid plexus. It mediated the uptake of T_3, T_4, and reverse T_3, as well as organic anions such as $E_2$17βG, cerivastatin, and TRO-S, suggesting its involvement in the membrane transport of these ligands in the brain capillary.

T_3 and its prohormone, T_4, are produced in the thyroid gland and released into the blood. T_3 plays an essential role in brain development via binding to specific nuclear receptors (thyroid hormone receptor) (25). Deficiency of thyroid hormones particularly during fetal and neonatal period in the brain causes mental retardation and cretinism (26, 27). T_3 is supplied to the brain and peripheral tissues as T_4 from which T_3 is enzymatically produced by type 2 iodothyronine deiodinase (D2) (25). Therefore, the brain uptake process of T_4 from the circulating blood is the first step in all subsequent reactions of thyroid hormone in the brain. Whether there is a specific transport mechanism(s) for T_4 in brain capillary endothelial cells remains controversial. The brain uptake of T_4 was saturable in dogs (28) but not in mice (29). Analysis of the transport and molecular properties of Oatp14 should help us resolve this.

Transfection of Oatp14 cDNA into HEK293 cells resulted in a marked increase in the uptake of T_4, as well as reverse T_3, an inactive metabolite of T_4 produced by type 3 iodothyronine deiodinase. Although the uptake of T_3 by Oatp14-expressed cells was significantly greater than that by vector-transfected cells (Table II), T_3 was extensively taken up by vector-transfected cells (Table II). Whether the uptake in vector-transfected cells is ascribed to specific transport system(s) for T_3 or passive diffusion remains unknown. The transport activity for T_3 exhibited by Oatp14, obtained by subtraction of the uptake by vector-transfected cells from that by Oatp14-expressed cells, was ~6-fold lower than that for T_4 and reverse T_3 by Oatp14 (Table II), although the chemical structures of T_3 and reverse T_3 are quite similar. The K_i value of T_3 for Oatp14 was 25-fold greater than that of T_4 (Table III), and this may result in apparent low transport activity for T_3 by Oatp14. Oatp14 can also mediate bidirectional transport, because the efflux of T_4 is facilitated in Oatp14-expressed cells (Fig. 4), and it is possible that Oatp14 is involved in both the uptake and efflux of its ligands through the brain capillary (*i.e.* BBB).

Involvement of Oatp14 in maintaining homeostasis of T_4 in the brain was also supported by the change in expression levels

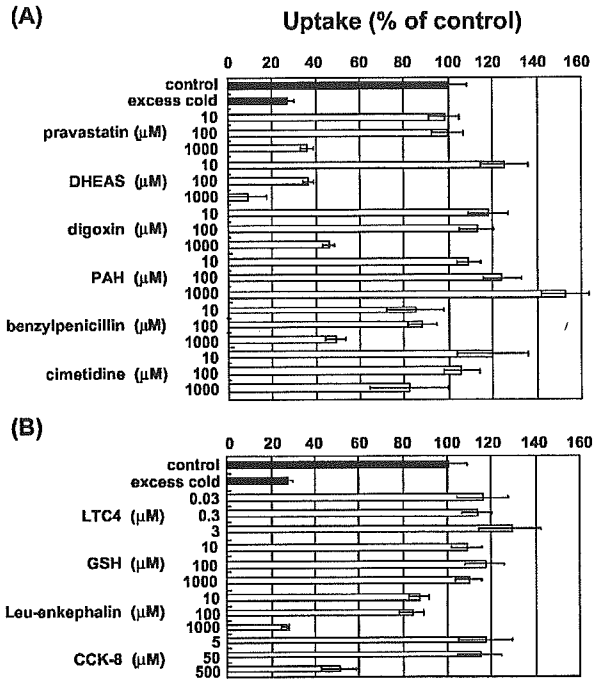

FIG. 6. **Effects of several unlabeled compounds on the uptake of [^{3}H]$E_2$17βG by Oatp14-transfected HEK293 cells.** The effects of several unlabeled compounds on the uptake of [^{3}H]$E_2$17βG by Oatp14-transfected HEK293 cells were examined at 37 °C. Results are given as a ratio with respect to the control values determined in the absence of unlabeled compounds. Each *point* represents the mean ± S.E. (n = 3). *DHEAS*, dehydroepiandrosterone sulfate; *PAH*, *p*-aminohippurate; *GSH*, glutathione; *CCK-8*, cholecystokinin-octapeptide.

TABLE III
K_i values for Oatp14

The K_i values were determined by nonlinear regression analysis using data shown in Fig. 5.

Inhibitor	K_i
	μM
Probenecid	39.5 ± 8.3
BSP	4.18 ± 1.02
Taurocholate	7.24 ± 3.33
ES	6.63 ± 1.62
DNP-SG	467 ± 67
DPDPE	86.3 ± 11.2
T3	2.46 ± 0.96
T4	0.11 ± 0.04

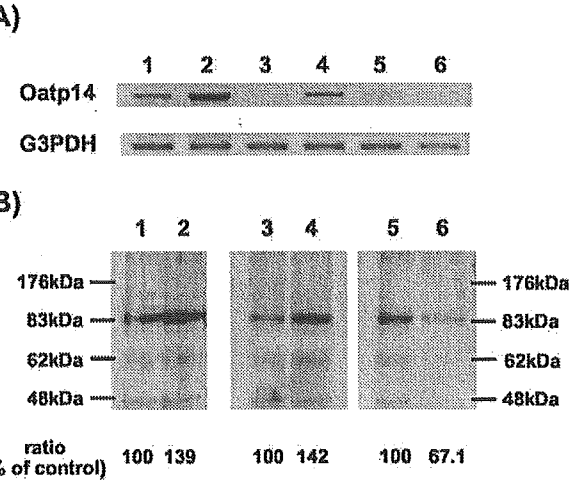

FIG. 7. **Effect of hyperthyroid and hypothyroid conditions on the expression of Oatp14 on the BBB.** *A*, RT-PCR analysis. mRNA samples were prepared from isolated brain capillary from control rats (*lanes 1*, *3*, and *5*), hypothyroid rats (MMI-treated or thyroidectomized rats; *lanes 2* and *4*, respectively) and hyperthyroid rats (T_3-treated rats; *lane 6*). PCR products stained with ethidium bromide were visualized under UV light. *G3PDH*, glucose-3-phosphate dehydrogenase. *B*, Western blotting. Brain capillaries (50 μg/*lane*) isolated from control rats (*lanes 1*, *3*, and *5*), hypothyroid rats (MMI-treated or thyroidectomized rats; *lanes 2* and *4*, respectively), and hyperthyroid rats (T_3-treated rats; *lane 6*) were separated by SDS-PAGE (10% separating gel). Oatp14 was detected by anti-Oatp14 polyclonal antibody.

of Oatp14 in the brain capillary under hypo- and hyperthyroid conditions (Fig. 7). The expression of Oatp14 in the brain capillary changed as if Oatp14 was responsible for maintaining the concentration of T_4 in the central nervous system: up- and down-regulated under hypothyroid and hyperthyroid conditions, respectively (Fig. 7). This pattern is similar to that observed in D2 expression (25). Increased D2 expression increases the conversion of T_4 to T_3 to compensate for the decrease in the local brain concentration of T_4 and vice versa. Therefore, we hypothesize that Oatp14 is involved in the uptake of T_4 through the brain capillaries.

In addition to Oatp14, Oatp2, the other isoform of rat Oatp family, is also the candidate transporter for T_3 and T_4 uptake by the brain from the circulating blood in rodents. The uptake of both T_3 and T_4 was significantly increased in Oatp2-cRNA injected oocytes with similar K_m values (~5–7 μM) (12). Oatp2 has been identified both in the luminal and abluminal membrane of brain capillary endothelial cells (15). It is possible that Oatp14 and Oatp2 serve high and low affinity sites for T_4 in the brain capillary, because the K_m values of Oatp2 were ~30-fold greater than that of Oatp14 (12). Following uptake from the circulating blood into endothelial cells, T_4 has to cross the abluminal membrane to reach the brain interstitial space and brain parenchymal cells. Whether this process is carrier-mediated remains unknown. Bidirectional nature of Oatp2-mediated transport has been reported in Oatp2-cRNA-injected oocytes (30). Oatp14 and Oatp2 are candidate transporters involved in the abluminal secretion of thyroid hormones. Further studies are necessary to identify the exact localization of Oatp14 in the brain capillary and to evaluate its contribution to the total brain uptake of T_4 into the brain. Pardridge *et al.* (31) demonstrated that the brain uptake of T_3 was saturable and inhibited by T_4 using carotid arterial bolus injection technique of Oldendorf, and Oatp2 may account for the brain uptake of T_3 in the brain capillary.

Oatp14 was detected in the choroid plexus by Western blot analysis (Fig. 1). The choroid plexus is located in the lateral, third and fourth ventricles, and the interface between the cerebrospinal fluid and the circulating blood acting as a barrier to protect the central nervous system, in conjunction with the BBB (32, 33). The brain distribution of T_3 and T_4 after intracerebroventricular administration is limited to ependymal cells and circumventricular organs and, thus, transport via the choroid plexus could account for the brain distribution near the ventricles (34). As speculated in the case of brain capillary endothelial cells, it is possible that Oatp14 acts as an uptake system to supply T_4 to ependymal cells and circumventricular organs in the choroid plexus.

In addition to thyroids, Oatp14 accepts certain types of amphipathic organic anions, such as $E_2$17βG, cerivastatin, and TRO-S, as substrates although their transport activity was markedly lower than that of T_4, except TRO-S (see Fig. 3 and Table II). Because Oatp14 can mediate the bidirectional trans-

port, it is possible that Oatp14 is involved in the efflux of organic anions such as $E_2 17\beta G$ from the brain when it is microinjected into the cerebral cortex and possibly in the efflux of excess T_4 and reverse T_3 from the brain. The spectrum of inhibitors of Oatp14 was consistent with the transporter hypothesized based on *in vivo* studies (18), but further investigations will be required to confirm this speculation.

Whether the results obtained using cDNA from rodents can be applied to the human situation is an important issue. Human OATP-F, an isoform in which Oatp14 exhibits high homology (84% in amino acid level), has a similar substrate specificity to Oatp14 (35). Northern blot analysis demonstrated abundant expression of OATP-F in the brain and testis and, to a lesser extent, heart, but the localization in the brain remains unidentified. In terms of substrate specificity and homology, OATP-F is supposed to be the human ortholog of Oatp14, and it may be suggested that OATP-F is also involved in the uptake of T_4 from the circulating blood into the central nervous system though the brain capillary and choroid plexus. In view of the importance of supplying T_4 to the brain during development, it is possible that functional loss of the OATP-F gene may be associated with a thyroid hormone-related neuronal disorder characterized by resistance to thyroid hormone treatment.

In conclusion, we have characterized Oatp14 in terms of its substrate specificity and localization in the brain and demonstrated that Oatp14 accepts T_4, as well as organic anions, including certain glucuronide and sulfate conjugates. Oatp14 is localized on the plasma membrane of brain capillary endothelial cells and involved in the uptake of T_4 from the blood to the central nervous system. Oatp14 is one of the mechanisms for maintaining homeostasis of T_4 and, ultimately, T_3 in the brain.

REFERENCES

1. Rapoport, S. I. (1976) *Exp. Neurol.* **52,** 467–479
2. Pardridge, W. M. (1991) *Semin. Cell Biol.* **2,** 419–426
3. Minn, A., Ghersi-Egea, J. F., Perrin, R., Leininger, B., and Siest, G. (1991) *Brain Res. Brain Res. Rev.* **16,** 65–82
4. Strazielle, N., and Ghersi-Egea, J. F. (1999) *J. Neurosci.* **15,** 6275–6289
5. Suzuki, H., Terasaki, T., and Sugiyama, Y. (1997) *Adv. Drug. Deliv. Rev.* **25,** 257–285
6. Kusuhara, H., and Sugiyama, Y. (2001) *Drug Discov. Today* **6,** 150–156
7. Lee, G., Dallas, M., Hong, M., and Bendayan, R. (2001) *Pharmacol. Rev.* **52,** 569–596
8. Kullak-Ublick, G. A., Stieger, B., Hagenbuch, B., and Meier, P. J. (2000) *Semin. Liver Dis.* **20,** 273–292
9. Kullak-Ublick, G. A., Ismair, M. G., Stieger, B., Landmann, L., Huber, R., Pizzagalli, F., Fattinger, K., Meier, P. J., and Hagenbuch. B. (2001) *Gastroenterology* **120,** 525–533
10. Jacquemin, E., Hagenbuch, B., Stieger, B., Wolkoff, A. W., and Meier, P. J. (1994) *Proc. Natl. Acad. Sci. U.S.A.* **91,** 133–137
11. Noe, B., Hagenbuch, B., Stieger, B., and Meier, P. J. (1997) *Proc. Natl. Acad. Sci. U. S. A.* **94,** 10346–11035
12. Abe, T., Kakyo, M., Sakagami, H., Tokui, T., Nishio, T., Tanemoto, M., Nomura, H., Hebert, S. C., Matsuno, S., Kondo, H., and Yawo, H. (1998) *J. Biol. Chem.* **273,** 22395–22401
13. Nishio, T., Adachi, H., Nakagomi, R., Tokui, T., Sato, E., Tanamoto, M., Fujiwara, K., Okabe, M., Onogawa, T., Suzuki, T., Nakai, D., Shiiba, K., Suzuki, M., Ohtani, H., Kondo, Y., Unno, M., Ito, S., Iinuma, K., Nunoki, K., Matsuno, S., and Abe, T. (2000) *Biochem. Biophys. Res. Commun.* **275,** 831–838
14. Kullak-Ublick, G. A., Hagenbuch, B., Stieger, B., Schteingart, C. D., Hofmann, A. F., Wolkoff, A. W., and Meier, P. J. (1995) *Gastroenterology* **109,** 1274–1282
15. Gao, B., Stieger, B., Noe, B., Fritschy, J. M., and Meier, P. J. (1999) *J. Histochem. Cytochem.* **47,** 1255–1264
16. Gao, B., Hagenbuch, B., Kullak-Ublick, G. A., Benke, D., Aguzzi, A., and Meier, P. J. (2000) *J. Pharmacol. Exp. Ther.* **294,** 73–79
17. Dagenais, C., Ducharme, J., and Pollack, G. M. (2001) *Neurosci. Lett.* **301,** 155–158
18. Sugiyama, D., Kusuhara, H., Shitara, Y., Abe, T., Meier, P. J., Sekine, T., Endou, H., Suzuki, H., and Sugiyama, Y. (2001) *J. Pharmacol. Exp. Ther.* **298,** 316–322
19. Li, J. Y., Boado, R., and Pardridge, W. M. (2001) *J. Cereb. Blood Flow Metab.* **21,** 61–68
20. Izumi, T., Hosiyama, K., Enomoto, S., Sasahara, K., and Sugiyama, Y. (1997) *J. Pharmacol. Exp. Ther.* **280,** 1392–40021
21. Akita, H., Suzuki, H., Ito, K., Kinoshita, S., Sato, N., Takikawa, H., and Sugiyama, Y. (2001) *Biochim. Biophys. Acta* **1511,** 7–16
22. Boado, R. J., and Pardridge, W. M. (1991) *J. Neurochem.* **57,** 2136–2139
23. Lowry, O. (1951) *J. Biol. Chem.* **193,** 265–273
24. Burmeister, L. A., Pachucki, J., and Germain, D. L. S. (1997) *Endocrinology* **138,** 5231–5237
25. Forrest, D., Reh, T. A., and Rusch, A. (2002) *Curr. Opin. Neurol.* **12,** 49–56
26. Oppenheimer, J. H., and Schwartz, H. L. (1997) *Endocr. Rev.* **18,** 462–475
27. Shi, Y. B., Ritchie, J. W. A., and Taylor, P. M. (2002) *Pharmacol. Ther.* **94,** 235–251
28. Hagen, G. A., and Solberg, L. A., Jr. (1974) *Endocrinology* **95,** 1398–1410
29. Banks, W. A., Kastin, A. J., and Micahls, E. A. (1985) *Life Sci.* **37,** 2407–2414
30. Li, L., Meier, P. J., and Ballatori, N. (2000) *Mol. Pharmacol.* **58,** 335–340
31. Pardridge, W. M. (1979) *Endocrinology* **105,** 605–612
32. Groothuis, D. R., and Levy, R. M. (1997) *J. Neurovirol.* **3,** 387–400
33. Segal, M. B. (2000) *Cell. Mol. Neurobiol.* **20,** 183–196
34. Dratman, M. B., Chrutchfield, F. L., and Schoenhoff, M. B. (1991) *Brain Res.* **554,** 229–236
35. Pizzagalli, F., Hagenbuch, B., Stieger, B., Klenk, U., Folkers, G., and Meier, P. J. (2002) *Mol. Endocrinol.* **16,** 2283–2296

[CANCER RESEARCH 63, 4882–4887, August 15, 2003]

Two Distinct Gene Expression Signatures in Pediatric Acute Lymphoblastic Leukemia with *MLL* Rearrangements[1]

Shuichi Tsutsumi, Takeshi Taketani, Kunihiro Nishimura, Xijin Ge, Tomohiko Taki, Kanji Sugita, Eiichi Ishii, Ryoji Hanada, Misao Ohki, Hiroyuki Aburatani, and Yasuhide Hayashi[2]

Genome Science Division, Research Center for Advanced Science and Technology, The University of Tokyo, Meguro-ku, Tokyo 153-8904 [S. T., X. G., H. A.]; Department of Pediatrics, Graduate School of Medicine [Ta. T., To. T., Y. H.] and School of Information Science and Technology, The University of Tokyo, Bunkyo-ku, Tokyo 113-8655 [K. N.]; Department of Pediatrics, Yamanashi Medical University, Tamaho-cho, Nakakoma-gun, Yamanashi 409-3898 [K. S.]; Department of Pediatrics, Saga Medical School, Saga 849-8501 [E. I.]; Division of Hematology/Oncology, Saitama Children's Medical Center, Iwatsuki, Saitama 339-8551 [R. H.]; and Cancer Genomics Division, National Cancer Center Research Institute, Chuo-ku, Tokyo 104-0045 [M. O.], Japan

ABSTRACT

Acute lymphoblastic leukemia (ALL) with 11q23 translocations is usually associated with *MLL* gene rearrangement, but little is known about its leukemogenesis. We analyzed the gene expression profiles of pediatric ALL samples according to their translocations. Using oligonucleotide microarray analysis, we identified distinct expression profiles for 23 ALL samples with 11q23 translocations, including t(4;11) (n = 15), t(11;19) (n = 6), and t(5;11) (n = 2), compared with 9 ALL samples with other translocations, including t(12;21) (n = 6) and t(1;19) (n = 3). Gene expression scores of *FLT3*, *MeisI*, and *CD44* for samples with *MLL* rearrangements were particularly high compared with those for other ALL samples. Statistical analysis of the gene expression profiles for the 21 ALL samples with *MLL* rearrangements at diagnosis revealed two subgroups that exclusively correlated with prognosis but not with any other clinico-pathological factor. The transcription factors *CBF2* and *CDP* were highly expressed in the poor and good prognosis subgroups, respectively. In addition, their downstream target genes were differentially expressed. These findings provide new insights into the biological mechanisms of leukemogenesis and prognosis for pediatric ALL with *MLL* rearrangements.

INTRODUCTION

The prognosis of children with ALL[3] has improved remarkably over the last 2 decades (1–3). This success has been achieved by using risk-directed therapy, which was developed after the realization that pediatric ALL is a heterogeneous disease (4). However, 20–25% of ALL patients still experience a relapse. Attempts to classify pediatric ALL into therapeutically relevant risk categories have relied mainly on clinical parameters, including age and WBC count at diagnosis, as well as early response to treatment (4). Recent advances in molecular biology have identified several genes involved in chromosomal translocations of ALL, such as the *E2A-PBX1* chimeric gene in t(1;19), *ETV6/TEL-AML1* in t(12;21), *BCR-ABL* in t(9;22), and *MLL-AF4* in t(4;11) (Refs. 1–5). Patients with t(12;21)-ALL have a good prognosis while those with t(9;22)- or t(4;11)-ALL have a poor prognosis. Infant ALL with *MLL* rearrangements (*MLL*-Re-ALL), including t(4;11) and t(11;19), is strongly associated with poor prognosis (6). Thus, cytogenetic or direct molecular genetic methods have become an essential part of the routine diagnosis and follow-up of acute leukemia patients, as well as increasing our understanding of leukemogenesis.

The *MLL* gene (also known as *ALL-1* or *HRX*), located at 11q23, encodes a protein of 3969 amino acids containing zinc fingers and AT-hook motifs and has homology with *Drosophila* trithorax protein (7–9). The *MLL* gene fuses with >30 genes on various partner chromosomes (10–12) and is highly conserved across species. Through its regulation of the *HOX* genes, *MLL* is essential for normal mammalian development and hematopoiesis. Although the function of the various *MLL* fusion genes and proteins is poorly understood, it appears that their fusion proteins disrupt the ability of wild-type *MLL* to regulate *HOX* gene expression, leading to leukemogenesis (13).

Recently, a genomic approach to cancer classification, including leukemia classification (14–17), based on gene expression monitoring using DNA microarrays, has been reported, with a distinct gene expression in pediatric T-ALL shown to be associated with a poor/good prognosis (17). *MLL*-Re-ALL has been reported to have characteristic, distinct gene expression profiles that are consistent with an early hematopoietic progenitor cell expressing selected multilineage markers and individual *HOX* genes. Clustering algorithms reveal that, based on their gene expression patterns, acute leukemia with *MLL* rearrangements can clearly be separated from conventional ALL and AML (18), suggesting that they constitute a distinct disease. Among *MLL*-Re-ALLs, infant patients have a poor prognosis. However, children > 1 years old have a relatively good prognosis (4). We used an oligonucleotide microarray to analyze the expression of >12,600 genes in leukemic cells from 31 pediatric ALL patients, including 15 with t(4;11), 6 with t(11;19), and 2 with t(5;11). We found that *MLL*-Re-ALL could be identified from the distinct expression pattern of several genes, including *FLT3*, *CD44*, *HOXA9*, and *MEIS1*. Furthermore, using the gene expression profiles, each of the t(4;11), t(11;19), or t(5;11) found in *MLL*-Re-ALL could be classified into two distinct groups, with differential prognosis, irrespective of their translocation partner chromosomes.

MATERIALS AND METHODS

Leukemia Samples. Leukemia cells from the bone marrow or peripheral blood of ALL patients were obtained with informed consent at diagnosis or relapse. In each case, the percentage of blasts was >90%. CD19 was expressed in all samples, but CD2, CD5, and CD7 were not expressed in any samples. We analyzed 32 ALL samples with chromosomal translocations, comprising 3 samples with t(1;19), 6 with t(12;21), and 23 with *MLL* rearrangements, including 15 t(4;11), 6 t(11;19), and 2 t(5;11). Samples were obtained both at diagnosis and relapse from one patient with t(4:11) and only at relapse from one *MLL*-Re-ALL sample. Therefore, the remaining 21 samples were obtained only at diagnosis. All of the translocations were subjected to karyotype analysis, fluorescence *in situ* hybridization, and/or Southern blot analyses, and *MLL* partner genes were confirmed by RT-PCR as described elsewhere (11, 19–21). The t(1;19), t(12;21), t(4;11), t(11;19), and t(5;11) samples were found

Received 3/25/03; revised 5/26/03; accepted 6/3/03.

The costs of publication of this article were defrayed in part by the payment of page charges. This article must therefore be hereby marked *advertisement* in accordance with 18 U.S.C. Section 1734 solely to indicate this fact.

[1] Supported by a grant-in-aid for Cancer Research from the Ministry of Health and Welfare of Japan, a grant-in-aid for Scientific Research on Priority Areas, and a grant-in-aid for Scientific Research (B) and (C) from the Ministry of Education, Culture, Sports, Science and Technology, Japan. This study was carried out as a part of The Technology Development for Analysis of Protein Expression and Interaction in Bioconsortia on R&D of New Industrial Science and Technology Frontiers, which was performed by The Industrial Science, Technology, and Environmental Policy Bureau and Ministry of Economy, Trade, and Industry and entrusted by The New Energy Development Organization.

[2] To whom requests for reprints should be addressed, at Department of Pediatrics, Graduate School of Medicine, The University of Tokyo, 7-3-1 Hongo, Bunkyo-ku, Tokyo 113-8655, Japan. E-mail: hayashiy-tky@umin.ac.jp.

[3] The abbreviations used are: ALL, acute lymphoblastic leukemia; AD, average difference; RT-PCR, reverse transcription-PCR; *HOX, homeobox*; AML, acute myeloid leukemia; TGF, transforming growth factor; PCA, principal component analysis; SVM, support vector machine.

to have *E2A-PBX1* (22), *TEL-AML1*, *MLL-AF4* (19), *MLL-ENL* (19), and *MLL-AF5q31* (11) fusion genes, respectively. Infant *MLL*-Re-ALL patients were mainly treated according to the MLL-96 protocol (23).

RNA Extraction and High-Density Oligonucleotide Array Analysis. Total RNA and genomic DNA were isolated from frozen cells using the ISOGEN reagent (Nippon Gene, Tokyo, Japan) according to the manufacturer's protocol. The quality of total RNA was examined by gel electrophoresis to confirm that the ribosomal 28S and 18S RNA bands were intact. The experimental procedures for GeneChip (Affymetrix, Santa Clara, CA) were performed according to the Affymetrix GeneChip expression analysis technical manual as described previously (24, 25). Briefly, 3–5 μg of total RNA were used to synthesize biotin-labeled cRNA, which was then hybridized to a GeneChip Human U95 V2 oligonucleotide array (Affymetrix). After washing, the arrays were stained with streptavidin-phycoerythrin and analyzed on a Hewlett-Packard Scanner to collect the image data. GeneChip Analysis Suite software 4.0 was used to calculate the AD for each gene probe set on the array, which was shown as an intensity value of the gene expression. The AD values were normalized for each array so that the average of all AD values was 100. Raw data are available on the Internet.[4]

Statistical Analysis. For each expression data set, where the AD values lay outside the range (10–8000), the value was reset to a minimum of 10 and a maximum of 8000. Subsequently, all values were log transformed for further analysis. Hierarchical clustering analysis was performed using GeneSpring (Silicon Genetics, Inc., Redwood, CA), CLUSTER, and TREEVIEW software (Eisen Lab.; Ref. 26).

Genes that correlated with particular class distinctions were identified as described by Golub *et al.* (14). We used the signal-to-noise statistic $(\mu_0 - \mu_1)/(\sigma_0 + \sigma_1)$, where μ and σ represent the mean and SD of expression, respectively, for each class. We also carried out 100,000 permutations of the samples by Mann-Whitney U and Kruskal-Wallis H tests to determine whether the correlations were more significant than would be expected by chance alone. Applying PCA, the coordinates of the first three principal components for each sample were selected. An SVM algorithm (27) was also applied to classify the samples using a modified version of the SVM light.

RT-PCR and Sequence Analysis. cDNA was reverse transcribed from 5 μg of total RNA using a cDNA synthesis kit (Invitrogen, Carlsbad, CA). PCR amplification was performed with the Advantage 2 PCR kit (Clontech, Palo Alto, CA) by incubating at 94°C for 2 min, followed by 35 cycles of 94°C for 30 s and 68°C for 2 min using *FLT3*-specific primers (F1; 5′-CCCAACTGCACAGAAGAGATCACAG-3′ and F2; 5′-TACAGCCTGTTAGGGATAGGTGGAGGG-3′). The PCR products were purified using a Qiaquick PCR purification kit (Qiagen, Hilden, Germany) and subjected to direct sequencing with primers (5′-CCAGCATGCCTGGTTCAAGAG-3′, 5′-GCCCTGAGATTTGATCCGAGTC-3′, 5′-GTGGGAAATCTTCTCACTTGG-3′, 5′-ATCCTAGTACCTTCCCAAACTC-3′, 5′-AGAGAGGCACTCATGTCAGAAC-3′, F1 and F2) using DYEnamic ET Terminator Kits (Amersham Biosciences, Piscataway, NJ) on an Applied Biosystems DNA sequencer. Internal tandem duplications of the *FLT3* gene were investigated by RT-PCR using the primers (5′-TGTCGAGCAGTACTCTAAACA-3′ and 5′-ATCCTAGTACCTTCCCAAACTC-3′) and electrophoresis as described previously (20).

Genomic PCR and Restriction Fragment-length Polymorphism Analysis. We amplified the exon 20 of the *FLT3* gene by genomic PCR using the primers (5′-GTTTGTTGCACATCATCATGGCCG-3′ and 5′-CCACAGTGAGTGCAGTTGTTTACCATG-3′) incubating at 94°C for 2 min, followed by 35 cycles of 94°C for 30 s and 68°C for 30 s. Amplified products were digested with *Eco*RV and subjected to electrophoresis on an agarose gel (Fig. 4).

RESULTS

Gene Expression Profiling Can Identify the Translocation Type in ALL Samples. We analyzed 32 pro-B or early pre-B ALL samples, including those with *MLL* rearrangements (n = 23), *TEL-AML1* (n = 6), and *E2A-PBX1* (n = 3), with Affymetrix oligonucleotide microarrays containing 12,600 probe sets. All samples showed high *CD19* expression signals. Relatively higher expression of *CD44* and lower of *CD10* (*MME*), *CD22*, *CD24*, and *CD79B* were found in patients with *MLL* rearrangements rather than in those with *TEL-AML1* and *E2A-PBX1* (supplementary information is available on the Internet).[4]

The results of the PCA were plotted with three-dimensional scaling to determine whether we could identify the ALL translocation types from their gene expression profiles. Samples carrying *MLL* rearrangements, those with *TEL-AML1* and *E2A-PBX1*, were resolved with this method. In contrast, no distinct subgroups were observed for defined *MLL* rearrangements, such as *MLL-ENL*, *MLL-AF4*, or *MLL-AF5q31* fusion genes (Fig. 1*A*). To classify the samples according to the similarity of their gene expression patterns and classify the genes according to the expression similarities over the samples, we applied a two-dimensional hierarchical clustering algorithm. In this analysis, samples with *TEL-AML1* and *E2A-PBX1* fusion were also subclassified into their respective clusters (Fig. 1*B*).

We next selected a list of genes whose expression patterns were

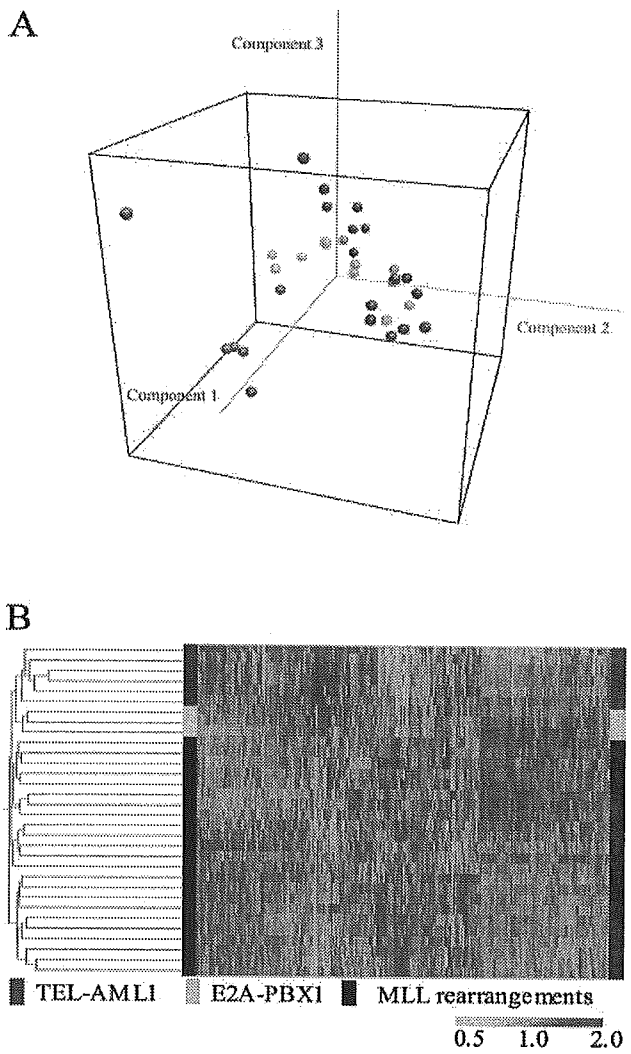

Fig. 1. *A*, comparison of gene expression in ALL associated with specific translocations. PCA plot of ALL with *TEL-AML1* fusion gene (*red*), *E2A-PBX2* (*yellow*), *MLL-AF4* (*blue*), *MLL-ENL* (*green*), and *MLL-AF5q31* (*purple*) carried out using 8322 genes that passed filtering. *B*, unsupervised two-dimensional hierarchical clustering analysis on ALL samples. This analysis was carried out using 3847 genes that passed filtering. Each *column* represents a gene and each *row* a sample. Relative expression levels are shown in *red* (relatively high) and *cyan* (relatively low).

[4] Internet address: http://www2.genome.rcast.u-tokyo.ac.jp/MLL.

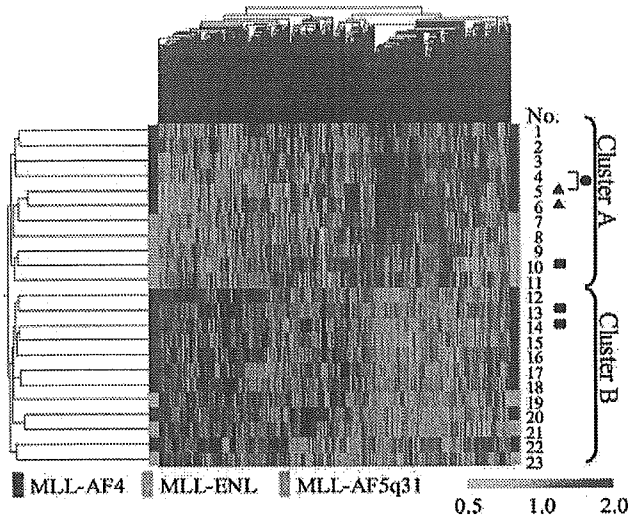

Fig. 2. Two-dimensional hierarchical clustering analysis on *MLL*-Re-ALL samples. Each *column* represents a gene and each *row* a sample. Relative expression levels are shown in *red* (relatively high) and *cyan* (relatively low). The *colored bar* on either side of the cluster identifies the fusion gene of each sample (*blue, MLL-AF4*; *green, MLL-ENL*; *purple, MLL-AF5q31*). ●, samples from the same patient. Two samples were taken at relapse (▲). Asp835 mutations were found in three samples (■).

correlated with particular translocations (*MLL* rearrangements, *E2A-PBX1* and *TEL-AML1*) using signal-to-noise analysis (supplementary Fig. 7; Ref. 14). Among 50 genes that were uniquely expressed in a subset of *MLL* rearrangements, 13 genes were also found in 50 unique genes for *MLL*-Re-ALL in a previous report (18). These included *LGALS1*, *CD44*, *CD45*, and *PMX1*. Furthermore, we found that *FLT3* and *MEIS1* were expressed highly, and *CD10* (*MME*) was less expressed in the samples with *MLL* rearrangements.

Two Distinct Patterns of Gene Expression among *MLL*-Re-ALL Samples. Gene expression patterns for leukemias with *MLL* rearrangements have been reported to be unique compared with those in other ALL without *MLL* rearrangements or AML (18). To investigate the variations in gene expression patterns among *MLL*-Re-ALL samples, we used a two-dimensional hierarchical clustering analysis on gene expression profiles for our 23 *MLL*-Re-ALL samples. This analysis produced two major sample clusters (Fig. 2). Two expression profiles generated from samples at onset and relapse from the same patient were classified in the same cluster. Excluding the two relapse samples, a random permutation test showed that the expression profiles of these two groups were statistically different ($P < 0.01$ by Mann-Whitney *U* test, see supplementary Fig. 9). Fourteen hundred of the 4200 genes expressed in this analysis showed distinct ($P < 0.05$) expression patterns between the two major clusters of *MLL*-Re-ALL samples. These probabilities were more significant than those between the two groups based on translocations (6 *MLL-ENL* samples *versus* 13 *MLL-AF4* samples). In fact, samples No. 20 and No. 21 carrying different *MLL*-partner genes had a correlation value of 0.49, which was much higher than the value of −0.07 found between samples No. 1 and No. 20 that have the same *MLL* partner gene. The two groups of patients were not significant in age or WBC counts at diagnosis (by Mann-Whitney *U* test), gender, or treatment (by χ^2 test; data not shown).

Gene Expression Signature Has Prognostic Relevance for *MLL*. To elucidate the possible clinical significance associated with the two main expression profile groups, Kaplan-Meier analysis was performed for relapse and survival (Fig. 3). Excluding the two samples obtained at relapse, Kaplan-Meier analysis showed that Cluster B in Fig. 2 was associated with a distinctly favorable prognosis. As shown in Fig. 3*B*, the overall probability of survival at 3 years was 92 ± 8% SE for Cluster B and 0% for Cluster A ($P = 0.0005$ by Log-rank analysis). The probability of event-free survival at 3 years was 73 ± 14% for Cluster B and 0% for Cluster A ($P = 0.01$). *MLL*-Re-ALL patients < 1 year old are reportedly associated with a poor prognosis, whereas those with t (4;11) and >1 year old have relatively good prognosis (2, 4, 6). In our study, only 1 patient (No. 22 on Fig. 2) was older than 1 year and subclassified in the favorable cluster B.

As reported previously (18), we found that *MLL*-Re-ALL is characterized by elevated levels of *FLT3* expression (shown in supplementary Fig. 8*A*). The AD values of *FLT3* showed no significant difference between the two clusters. Internal tandem duplication of the *FLT3* gene has been reported in 20–30% of adult AML (28, 29) and 15% of childhood AML (30). In addition, mutations of the *FLT3* gene have been reported in 5% of adult AML (31). We investigated Asp835 mutations of the *FLT3* gene by direct sequence and restriction fragment-length polymorphism analysis of genomic PCR products. Three (14%) of 21 *MLL*-Re-ALL patients, 1 from Cluster A and 2 from Cluster B, were found to have Asp835 mutations (Fig. 4). This was confirmed by sequence analysis of *FLT3* cDNA. No other mutations were found in the intracellular region of *FLT3* by sequence analysis of

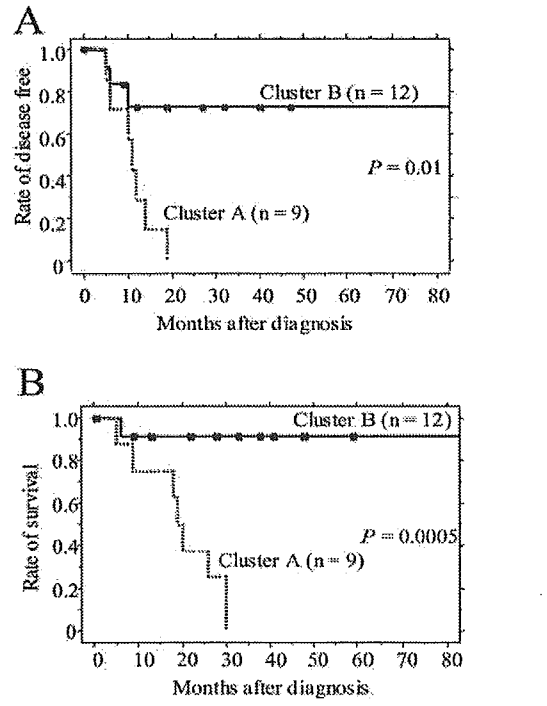

Fig. 3. Survival analysis of *MLL*-Re-ALL. Kaplan-Meier curves for Cluster A ($n = 9$) *versus* Cluster B ($n = 12$). *A*, disease-free survival; *B*, overall survival.

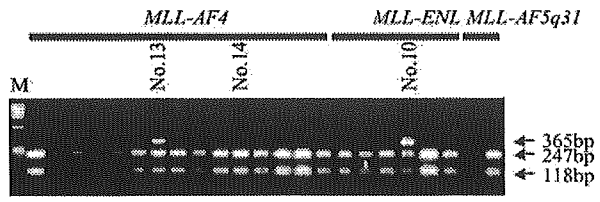

Fig. 4. Detection of Asp835 mutation of the *FLT3* gene. The *arrow* (*356 bp*) indicates Asp835 mutation of the *FLT3* gene. The *lane numbers* correspond to the sample numbers in Fig. 2.

cDNA. RT-PCR analysis failed to reveal internal tandem duplications of the *FLT3* in any of the samples (data not shown).

Biological Aspects between the Two Differential Prognostic Clusters. To investigate the biological features of the two clusters shown in Fig. 2, signal:noise expression ratios were calculated for the two groups as described previously (14), and the top and bottom 30 ranked genes that differentiated between the two groups were selected (Fig. 5). Transcription factors/coactivators were found among the top 30 discriminating genes for both clusters. In Cluster A (Gene list U), *TRIP3* and *CBF2*, and in Cluster B (gene list F), *CDP*, *NCOR1*, *USF2*, *ZFP36L2*, and *SMARCC2* were found among the top discriminating genes. We compared the promoter targets for these transcription factors with the upstream promoter sequences of other genes in our lists. CDP was reported to bind to at least two homeotic CCAAT motifs located upstream of the TATA element and to suppress histone gene expression (32). Four of the genes in gene list U (*TRIP3*, *H2BFL*, *C14orf2*, and *MDH1*), with expression suppressed in samples with elevated *CDP* expression, have two 5′-CCAAT-3′ motifs (5′-CCAAT-3′-53–72 bp-5′-CCAAT-3′), located between 500 bp upstream and 100 bp downstream of the transcription start site. This indicates that the expression patterns of these genes may be functionally related.

The precise subclassification of unknown samples into the two clusters by gene expression profiling is especially important in *MLL*-Re-ALL because there are few conventional methods for predicting the prognosis of those types of ALL. A supervised SVM was used against these higher and lower signal-to-noise genes to classify the samples. The test sample was classified using a leave-one-out model for the remaining 20 samples. Through all 21 cycles, 100% accuracy in predicting prognosis was achieved with between 21 and 1000 genes selected for higher or lower signal-to-noise values (data not shown). This result suggested that the prognosis of *MLL*-Re-ALL could be predicted reliably by using the expression profiles of selected genes.

DISCUSSION

To make an accurate diagnosis of pediatric ALL, many clinical diagnostic examinations are required. It is necessary to consider the interrelationship of various prognostic factors, including chromosomal translocations (1, 2, 4, 12). ALL patients with t (12;21; *TEL-AML1*) are associated with a good clinical outcome (2, 4), whereas *MLL*-Re-ALL patients are associated with a poor outcome (1, 2, 4, 10, 12). Our data suggest that *MLL*-Re-ALL can be diagnosed from gene expression profiles. *FLT3*, *MEIS1*, and the 13 genes reported previously (18) were also found in the top 50 genes expressed highly in our *MLL*-Re-ALL samples. *HOXA9*, a heterodimer partner of *MEIS1*, was significantly expressed in *MLL*-Re-ALL samples ($P < 0.05$ by Mann-Whitney *U* test).

One of the most interesting findings in this study was the remarkable variance in the gene expression signatures of *MLL*-Re-ALL. This difference was more significant than that between 13 samples with t t(4;11) and 6 with t(11;19). This result strongly suggests that at least two subgroups exist in *MLL*-Re-ALL independent of the *MLL* partner genes, with patients in one subgroup (Cluster A) having a remarkably poor prognosis.

It was reported that an internal tandem duplication of *FLT3* in AML predicted poor prognosis, and recently, mutations of *FLT3* have been reported to be rare in AML (31). Our result showed Asp835 mutations of *FLT3* in 3 (14%) of 21 *MLL*-Re-ALL patients, but we found no tandem duplications of *FLT3* similar to our previous report (20). Elevated expression of the *FLT3* gene was not associated with either cluster, and Asp835 mutations were not associated with prognosis. Except for *SPN*, expression of these leukocyte markers, *CD10*, *CD19*, CD22, *CD24*, *CD44*, *CD79B*, and *TdT*, were not significantly correlated with the two clusters (supplementary Fig. 6). It was reported that, with intensive treatment, including hematopoietic stem cell transplantation, 30–40% of *MLL*-Re-ALL infants remained free of relapse

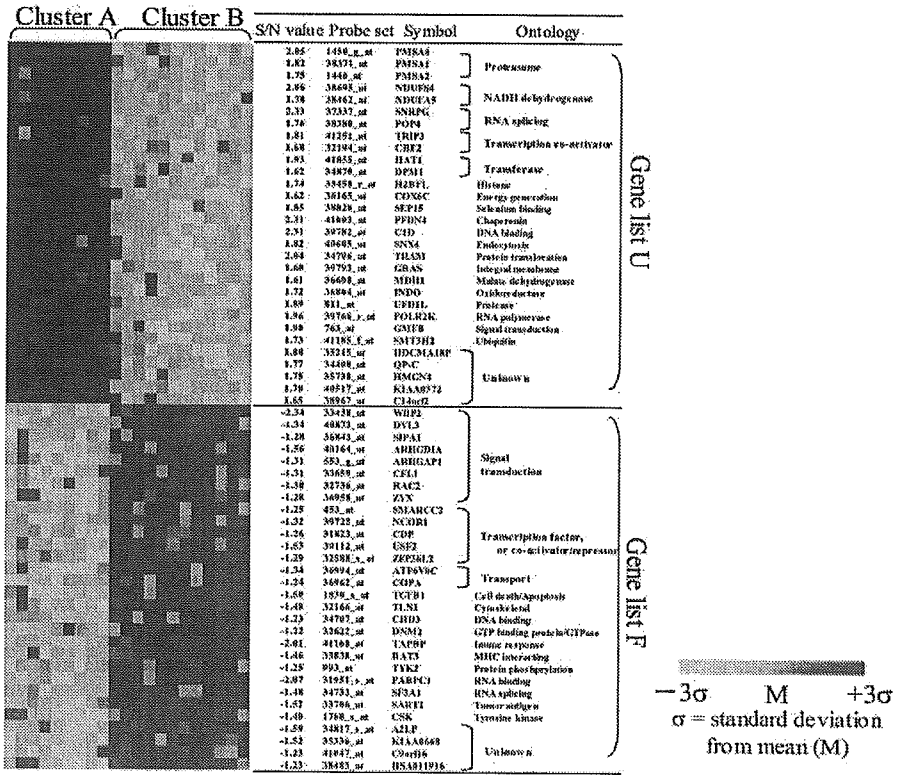

Fig. 5. Genes specifically expressed in Cluster A or Cluster B. The top 30 genes (Gene list U) and bottom 30 genes (Gene list F) by signal-to-noise values are shown. Each *column* represents a leukemia sample and each *row* a gene. The signal-to-noise value (S/N value) for the probe set of U95A array, gene symbol, and gene ontology is shown on the *right*. In each gene list, the genes are arranged according to their ontologies. Relative expression levels are shown in *red* (high) and *cyan* (low).

(4, 23, 33, 34), suggesting the existence of two patient groups with differential prognosis. Our results demonstrate that gene expression profiling is able to predict the prognosis of these distinct groups of *MLL*-Re-ALL more accurately than the conventional methods, such as karyotype analysis.

The top 30 and bottom 30 genes that were differently expressed between the two clusters (Clusters A and B) provided us with an insight into the biological behavior of ALL. In Gene list U, we found the transcriptional co-activators *TRIP3* and *CBF2*. *CBF2* was reported as a co-activator of NF-Y, which also bound the CCAAT motif (35–38). On the other hand, *CDP* (in Gene list F) also recognizes the CCAAT motif (32). CDP plays an essential role in the differentiation of hematopoietic cells (39). Loss of heterozygosity and reduced *CDP* expression has been observed in human uterine leiomyoma and breast cancer, providing the first evidence that CDP can act as a potential a tumor suppressor (40, 41). Our analysis of the promoter sites of the listed 60 genes suggested that CDP might suppress the expression of four genes in Cluster B samples. The transcription factors, CBF2 and CDP, may regulate the expression of, and be correlated quantitatively with, many genes that were differently expressed between the two clusters. For example, CBF2 was reported to induce *CDC2*, which has tandem CCAAT motifs in its promoter site (37, 42). Actually, *CDC2* showed a higher expression in Cluster A samples ($P < 0.05$ by unpaired t-test).

In the 30 genes expressed highly in Cluster B, we found 8 signal transduction genes, including four Rho family genes (*RAC2*, *ARHGDIA*, *ARHGAP1/GRAF*, and *CFL1*) and two GTP-associated genes (*DNM2* and *SIPA1*). This result suggests that different pathways are activated in Cluster B. *ARHGAP1/GRAF* is one of the partner genes of *MLL* (46). Biallelelic mutations of the *ARHGAP1/GRAF* gene have been identified in samples of myelodysplastic syndrome and AML. Recent studies have confirmed the oncogenic potential of Rho proteins (47, 48), and several studies suggest that Rho GTPases might be overfunctional in human cancers (49). It seems probable that the Rho pathway plays some roles in the leukemogenesis of patients with Cluster B.

In conclusion, these different gene expressions between the subgroups provided us with valuable information for clarifying the mechanism of leukemogenesis in *MLL*-Re-ALL. Further analysis of *MLL*-Re-ALL should lead to more accurate characterization of the key molecules of leukemogenesis and help in the search for new drug targets and diagnostic markers.

ACKNOWLEDGMENTS

We thank Shoko Sohma, Hisae Soga, Hiroko Meguro, Daisuke Komura and Shogo Yamamoto for their excellent technical assistance, Sigeo Ihara, Michael H. Jones and Yoshitaka Hippo for their excellent comments. We also thank Drs. Akira Morimoto, Masahiro Sako and all of the participants in the Japan Infant Leukemia Study Group for providing samples and clinical data.

REFERENCES

1. Kersey, J. H. Fifty years of studies of the biology and therapy of childhood leukemia. Blood, *90:* 4243–4251, 1997.
2. Pui, C. H., and Evans, W. E. Acute lymphoblastic leukemia. N. Engl. J. Med., *339:* 605–615, 1998.
3. Silverman, L. B., Gelber, R. D., Dalton, V. K., Asselin, B. L., Barr, R. D., Clavell, L. A., Hurwitz, C. A., Moghrabi, A., Samson, Y., Schorin, M. A., Arkin, S., Declerck, L., Cohen, H. J., and Sallan, S. E. Improved outcome for children with acute lymphoblastic leukemia: results of Dana-Farber Consortium Protocol 91-01. Blood, *97:* 1211–1218, 2001.
4. Pui, C. H., Campana, D., and Evans, W. E. Childhood acute lymphoblastic leukaemia–current status and future perspectives. Lancet Oncol., *2:* 597–607, 2001.
5. Look, A. T. Oncogenic transcription factors in the human acute leukemias. Science (Wash. DC), *278:* 1059–1064, 1997.
6. Taki, T., Ida, K., Bessho, F., Hanada, R., Kikuchi, A., Yamamoto, K., Sako, M., Tsuchida, M., Seto, M., Ueda, R., and Hayashi, Y. Frequency and clinical significance of the MLL gene rearrangements in infant acute leukemia. Leukemia (Baltimore), *10:* 1303–1307, 1996.
7. Gu, Y., Nakamura, T., Alder, H., Prasad, R., Canaani, O., Cimino, G., Croce, C. M., and Canaani, E. The t(4;11) chromosome translocation of human acute leukemias fuses the ALL-1 gene, related to Drosophila trithorax, to the AF-4 gene. Cell, *71:* 701–708, 1992.
8. Tkachuk, D. C., Kohler, S., and Cleary, M. L. Involvement of a homolog of Drosophila trithorax by 11q23 chromosomal translocations in acute leukemias. Cell, *71:* 691–700, 1992.
9. Djabali, M., Selleri, L., Parry, P., Bower, M., Young, B. D., and Evans, G. A. A trithorax-like gene is interrupted by chromosome 11q23 translocations in acute leukaemias. Nat. Genet., *2:* 113–118, 1992.
10. Rowley, J. D. The critical role of chromosome translocations in human leukemias. Annu. Rev. Genet., *32:* 495–519, 1998.
11. Taki, T., Kano, H., Taniwaki, M., Sako, M., Yanagisawa, M., and Hayashi, Y. AF5q31, a newly identified *AF4*-related gene, is fused to *MLL* in infant acute lymphoblastic leukemia with ins(5;11)(q31;q13q23). Proc. Natl. Acad. Sci. USA, *96:* 14535–14540, 1999.
12. Hayashi, Y. The molecular genetics of recurring chromosome abnormalities in acute myeloid leukemia. Semin. Hematol., *37:* 368–380, 2000.
13. Yu, B. D., Hess, J. L., Horning, S. E., Brown, G. A., and Korsmeyer, S. J. Altered *Hox* expression and segmental identity in Mll-mutant mice. Nature (Lond.), *378:* 505–508, 1995.
14. Golub, T. R., Slonim, D. K., Tamayo, P., Huard, C., Gaasenbeek, M., Mesirov, J. P., Coller, H., Loh, M. L., Downing, J. R., Caligiuri, M. A., Bloomfield, C. D., and Lander, E. S. Molecular classification of cancer: class discovery and class prediction by gene expression monitoring. Science (Wash. DC), *286:* 531–537, 1999.
15. Alizadeh, A. A., Eisen, M. B., Davis, R. E., Ma, C., Lossos, I. S., Rosenwald, A., Boldrick, J. C., Sabet, H., Tran, T., Yu, X., Powell, J. I., Yang, L., Marti, G. E., Moore, T., Hudson, J., Jr., Lu, L., Lewis, D. B., Tibshirani, R., Sherlock, G., Chan, W. C., Greiner, T. C., Weisenburger, D. D., Armitage, J. O., Warnke, R., Staudt, L. M., *et al.* Distinct types of diffuse large B-cell lymphoma identified by gene expression profiling. Nature, *403:* 503–511, 2000.
16. Yeoh, E. J., Ross, M. E., Shurtleff, S. A., Williams, W. K., Patel, D., Mahfouz, R., Behm, F. G., Raimondi, S. C., Relling, M. V., Patel, A., Cheng, C., Campana, D., Wilkins, D., Zhou, X., Li, J., Liu, H., Pui, C. H., Evans, W. E., Naeve, C., Wong, L., and Downing, J. R. Classification, subtype discovery, and prediction of outcome in pediatric acute lymphoblastic leukemia by gene expression profiling. Cancer Cell, *1:* 133–143, 2002.
17. Ferrando, A. A., Neuberg, D. S., Staunton, J., Loh, M. L., Huard, C., Raimondi, S. C., Behm, F. G., Pui, C. H., Downing, J. R., Gilliland, D. G., Lander, E. S., Golub, T. R., and Look, A. T. Gene expression signatures define novel oncogenic pathways in T cell acute lymphoblastic leukemia. Cancer Cell, *1:* 75–87, 2002.
18. Armstrong, S. A., Staunton, J. E., Silverman, L. B., Pieters, R., den Boer, M. L., Minden, M. D., Sallan, S. E., Lander, E. S., Golub, T. R., and Korsmeyer, S. J. *MLL* translocations specify a distinct gene expression profile that distinguishes a unique leukemia. Nat. Genet., *30:* 41–47, 2002.
19. Ida, K., Taki, T., Bessho, F., Kobayashi, M., Taira, F., Hanada, R., Yamamoto, K., Okimoto, Y., Seto, M., Ueda, R., and Hayashi, Y. Detection of chimeric mRNAs by reverse transcriptase-polymerase chain reaction for diagnosis and monitoring of acute leukemias with 11q23 abnormalities. Med. Pediatr. Oncol., *28:* 325–332, 1997.
20. Xu, F., Taki, T., Eguchi, M., Kamada, N., Ishii, E., Endo, M., and Hayashi, Y. Tandem duplication of the *FLT3* gene is infrequent in infant acute leukemia. Japan Infant Leukemia Study Group. Leukemia (Baltimore), *14:* 945–947, 2000.
21. Jamal, R., Taketani, T., Taki, T., Bessho, F., Hongo, T., Hamaguchi, H., Horiike, S., Taniwaki, M., Hanada, R., Nakamura, H., and Hayashi, Y. Coduplication of the MLL and FLT3 genes in patients with acute myeloid leukemia. Genes Chromosomes Cancer, *31:* 187–190, 2001.
22. Kawamura, M., Kikuchi, A., Kobayashi, S., Hanada, R., Yamamoto, K., Horibe, K., Shikano, T., Ueda, K., Hayashi, K., Sekiya, T., and Hayashi, Y. Mutations of the p53 and ras genes in childhood t(1;19)-acute lymphoblastic leukemia. Blood, *85:* 2546–2552, 1995.
23. Isoyama, K., Eguchi, M., Hibi, S., Kinukawa, N., Ohkawa, H., Kawasaki, H., Kosaka, Y., Oda, T., Oda, M., Okamura, T., Nishimura, S., Hayashi, Y., Mori, T., Imaizumi, M., Mizutani, S., Tsukimoto, I., Kamada, N., and Ishii, E. Risk-directed treatment of infant acute lymphoblastic leukaemia based on early assessment of *MLL* gene status: results of the Japan Infant Leukaemia Study (MLL96). Br. J. Haematol., *118:* 999–1010, 2002.
24. Ishii, M., Hashimoto, S., Tsutsumi, S., Wada, Y., Matsushima, K., Kodama, T., and Aburatani, H. Direct comparison of GeneChip and SAGE on the quantitative accuracy in transcript profiling analysis. Genomics, *68:* 136–143, 2000.
25. Hippo, Y., Taniguchi, H., Tsutsumi, S., Machida, N., Chong, J. M., Fukayama, M., Kodama, T., and Aburatani, H. Global gene expression analysis of gastric cancer by oligonucleotide microarrays. Cancer Res., *62:* 233–240, 2002.
26. Eisen, M. B., Spellman, P. T., Brown, P. O., and Botstein, D. Cluster analysis and display of genome-wide expression patterns. Proc. Natl. Acad. Sci. USA, *95:* 14863–14868, 1998.
27. Vapnik, V., and Chapelle, O. Bounds on error expectation for support vector machines. Neural Comput., *12:* 2013–2036, 2000.
28. Nakao, M., Yokota, S., Iwai, T., Kaneko, H., Horiike, S., Kashima, K., Sonoda, Y., Fujimoto, T., and Misawa, S. Internal tandem duplication of the flt3 gene found in acute myeloid leukemia. Leukemia (Baltimore), *10:* 1911–1918, 1996.
29. Hayakawa, F., Towatari, M., Kiyoi, H., Tanimoto, M., Kitamura, T., Saito, H., and Naoe, T. Tandem-duplicated Flt3 constitutively activates STAT5 and MAP kinase

and introduces autonomous cell growth in IL-3-dependent cell lines. Oncogene, *19:* 624–631, 2000.
30. Xu, F., Taki, T., Yang, H. W., Hanada, R., Hongo, T., Ohnishi, H., Kobayashi, M., Bessho, F., Yanagisawa, M., and Hayashi, Y. Tandem duplication of the *FLT3* gene is found in acute lymphoblastic leukaemia as well as acute myeloid leukaemia but not in myelodysplastic syndrome or juvenile chronic myelogenous leukaemia in children. Br. J. Haematol., *105:* 155–162, 1999.
31. Yamamoto, Y., Kiyoi, H., Nakano, Y., Suzuki, R., Kodera, Y., Miyawaki, S., Asou, N., Kuriyama, K., Yagasaki, F., Shimazaki, C., Akiyama, H., Saito, K., Nishimura, M., Motoji, T., Shinagawa, K., Takeshita, A., Saito, H., Ueda, R., Ohno, R., and Naoe, T. Activating mutation of D835 within the activation loop of FLT3 in human hematologic malignancies. Blood, *97:* 2434–2439, 2001.
32. Wu, F., and Lee, A. S. CDP and AP-2 mediated repression mechanism of the replication-dependent hamster histone H3.2 promoter. J. Cell. Biochem., *84:* 699–707, 2002.
33. Pui, C. H., Gaynon, P. S., Boyett, J. M., Chessells, J. M., Baruchel, A., Kamps, W., Silverman, L. B., Biondi, A., Harms, D. O., Vilmer, E., Schrappe, M., and Camitta, B. Outcome of treatment in childhood acute lymphoblastic leukaemia with rearrangements of the 11q23 chromosomal region. Lancet, *359:* 1909–1915, 2002.
34. Chessells, J. M., Harrison, C. J., Kempski, H., Webb, D. K., Wheatley, K., Hann, I. M., Stevens, R. F., Harrison, G., and Gibson, B. E. Clinical features, cytogenetics and outcome in acute lymphoblastic and myeloid leukaemia of infancy: report from the MRC Childhood Leukaemia working party. Leukemia (Baltimore), *16:* 776–784, 2002.
35. Lum, L. S., Sultzman, L. A., Kaufman, R. J., Linzer, D. I., and Wu, B. J. A cloned human CCAAT-box-binding factor stimulates transcription from the human hsp70 promoter. Mol. Cell. Biol., *10:* 6709–6717, 1990.
36. Mantovani, R. A survey of 178 NF-Y binding CCAAT boxes. Nucleic Acids Res., *26:* 1135–1143, 1998.
37. Kao, C. Y., Tanimoto, A., Arima, N., Sasaguri, Y., and Padmanabhan, R. Transactivation of the human cdc2 promoter by adenovirus E1A. E1A induces the expression and assembly of a heteromeric complex consisting of the CCAAT box binding factor, CBF/NF-Y, and a 110-kDa DNA-binding protein. J. Biol. Chem., *274:* 23043–23051, 1999.
38. Imbriano, C., Bolognese, F., Gurtner, A., Piaggio, G., and Mantovani, R. HSP-CBF is an NF-Y-dependent coactivator of the heat shock promoters CCAAT boxes. J. Biol. Chem., *276:* 26332–26339, 2001.
39. Sinclair, A. M., Lee, J. A., Goldstein, A., Xing, D., Liu, S., Ju, R., Tucker, P. W., Neufeld, E. J., and Scheuermann, R. H. Lymphoid apoptosis and myeloid hyperplasia in CCAAT displacement protein mutant mice. Blood, *98:* 3658–3667, 2001.
40. Neville, P. J., Thomas, N., and Campbell, I. G. Loss of heterozygosity at 7q22 and mutation analysis of the CDP gene in human epithelial ovarian tumors. Int. J. Cancer, *91:* 345–349, 2001.
41. Zeng, W. R., Scherer, S. W., Koutsilieris, M., Huizenga, J. J., Filteau, F., Tsui, L. C., and Nepveu, A. Loss of heterozygosity and reduced expression of the CUTL1 gene in uterine leiomyomas. Oncogene, *14:* 2355–2365, 1997.
42. Tanimoto, A., Chen, H., Kao, C. Y., Moran, E., Sasaguri, Y., and Padmanabhan, R. Transactivation of the human cdc2 promoter by adenovirus E1A in cycling cells is mediated by induction of a 110-kDa CCAAT-box-binding factor. Oncogene, *17:* 3103–3114, 1998.
43. Borkhardt, A., Bojesen, S., Haas, O. A., Fuchs, U., Bartelheimer, D., Loncarevic, I. F., Bohle, R. M., Harbott, J., Repp, R., Jaeger, U., Viehmann, S., Henn, T., Korth, P., Scharr, D., and Lampert, F. The human GRAF gene is fused to MLL in a unique t(5;11)(q31;q23) and both alleles are disrupted in three cases of myelodysplastic syndrome/acute myeloid leukemia with a deletion 5q. Proc. Natl. Acad. Sci. USA, *97:* 9168–9173, 2000.
44. Boerner, J. L., Danielsen, A., McManus, M. J., and Maihle, N. J. Activation of Rho is required for ligand-independent oncogenic signaling by a mutant epidermal growth factor receptor. J. Biol. Chem., *276:* 3691–3695, 2001.
45. van Golen, K. L., Wu, Z. F., Qiao, X. T., Bao, L. W., and Merajver, S. D. RhoC GTPase, a novel transforming oncogene for human mammary epithelial cells that partially recapitulates the inflammatory breast cancer phenotype. Cancer Res., *60:* 5832–5838, 2000.
46. Jordan, P., Brazao, R., Boavida, M. G., Gespach, C., and Chastre, E. Cloning of a novel human Rac1b splice variant with increased expression in colorectal tumors. Oncogene, *18:* 6835–6839, 1999.

THE JOURNAL OF BIOLOGICAL CHEMISTRY
Vol. 278, No. 40, Issue of October 3, pp. 38796–38802, 2003
Printed in U.S.A.

A Novel Mitochondrial Carnitine-acylcarnitine Translocase Induced by Partial Hepatectomy and Fasting*

Received for publication, June 16, 2003, and in revised form, July 24, 2003
Published, JBC Papers in Press, July 25, 2003, DOI 10.1074/jbc.M306372200

Ei Sekoguchi‡§¶, Norihiro Sato‖, Akihiro Yasui§, Shinji Fukada§, Yuji Nimura¶, Hiroyuki Aburatani, Kyoji Ikeda‡, and Akira Matsuura‡ ‡‡**

*From the ‡Department of Geriatric Research, National Institute for Longevity Sciences, Obu, Aichi 474-8522, Japan, the §Chubu National Hospital, Obu, Aichi 474-8522, Japan, the ¶Nagoya University Graduate School of Medicine, Showa-ku, Nagoya 466-8550, Japan, the ‖Tokyo University of Pharmacy and Life Science, Hachioji 192-0392, Japan, and the **Research Center for Advanced Science and Technology, University of Tokyo, Meguro-ku, Tokyo 153-8904, Japan*

The carnitine-dependent transport of long-chain fatty acids is essential for fatty acid catabolism. In this system, the fatty acid moiety of acyl-CoA is transferred enzymatically to carnitine, and the resultant product, acylcarnitine, is imported into the mitochondrial matrix through a transporter named carnitine-acylcarnitine translocase (CACT). Here we report a novel mammalian protein homologous to CACT. The protein, designated as CACL (CACT-like), is localized to the mitochondria and has palmitoylcarnitine transporting activity. The tissue distribution of CACL is similar to that of CACT; both are expressed at a higher level in tissues using fatty acids as fuels, except in the brain, where only CACL is expressed. In addition, CACL is induced by partial hepatectomy or fasting. Thus, CACL may play an important role cooperatively with its homologue CACT in a stress-induced change of lipid metabolism, and may be specialized for the metabolism of a distinct class of fatty acids involved in brain function.

Long-chain polyunsaturated fatty acids, such as arachidonic acid and docosahexaenoic acid, are important nutritional components, serving as structural elements in mammalian cells. They confer fluidity, flexibility, and selective permeability to cellular membranes, and affect cellular and physiological processes (1). In addition, long-chain fatty acids are used as an energy source through the mitochondrial β-oxidation pathway, especially in tissues such as muscle, during periods of fasting and other metabolic stress (2).

The carnitine shuttle system in eukaryotic cells provides for the entry of long-chain fatty acids into the mitochondrial matrix, where β-oxidation takes place (3, 4). Acyl-CoA pools supply activated substrates for many key metabolic pathways, such as the tricarboxylic acid cycle and lipid synthesis. A wide range of activated acyl groups is transferred reversibly from acyl-CoA to carnitine through the actions of carnitine acyltransferases. The transfer from the limited pools of membrane-impermeable CoA to the abundant and mobile carnitine allows transport between compartments.

Acylcarnitines are imported into mitochondria through carnitine-acylcarnitine translocase (CACT)[1] (5, 6). This protein catalyzes a mole to mole exchange of carnitines and acylcarnitines, thereby permitting the fatty acid moieties to be translocated into the mitochondrial matrix. Several cases of CACT deficiency have been reported (7–9). Patients with these defects generally present in early infancy with acute, potentially life-threatening episodes of hypoketotic hypoglycemic coma, induced by fasting during intercurrent disease. The clinical features of these patients include hypoketotic hypoglycemia, mild hyperammonemia, variable dicarboxylic aciduria, hepatomegaly with abnormal liver functions, various cardiac symptoms, and skeletal muscle weakness.

In a search for genes that are up-regulated during liver regeneration after partial hepatectomy in rodents, we found a novel gene that encodes a protein homologous to CACT. Here we report the characterization of the gene product, CACL (for carnitine-acylcarnitine translocase-like). The protein exhibits a mitochondrial carnitine-acylcarnitine translocase activity, and its expression is induced by stresses such as hepatectomy and fasting.

EXPERIMENTAL PROCEDURES

Animals—Eight-week-old C57BL/6J male mice were purchased from CLEA Japan Inc. (Tokyo, Japan). Animals were kept in a temperature-controlled animal room with a 12-h dark/light cycle and were maintained on a commercially available diet (CE-2, CLEA Japan Inc.) consisting (by energy) of 29.2% protein, 58.8% carbohydrates, and 12.0% fat. Mice were either fed *ad libitum* or fasted for 48 h, and had free access to water. A 70% partial hepatectomy was performed according to the method of Higgins and Anderson (10). The surgery was performed between 8 and 11 a.m. under ether anesthesia. Animals were sacrificed before partial hepatectomy and at 6, 12, 24, and 48 h after the operation. Hearts, livers, brains, and kidneys were excised, immediately frozen in liquid nitrogen, and stored at −80 °C. All experiments were conducted in accordance with the animal care guidelines of the National Institute for Longevity Sciences (Obu, Japan).

Cell Lines and Culture Conditions—NIH3T3 murine fibroblasts were maintained as monolayer cultures in Dulbecco's modified minimal essential medium (Sigma) supplemented with 10% (v/v) fetal bovine serum (ICN Biomedicals Inc., Aurora, OH), penicillin (100 units/ml), and streptomycin (100 μg/ml; Invitrogen Corp.) at 37 °C in a humidified atmosphere containing 95% air and 5% CO_2. The GP2-293 retroviral packaging cell line was obtained from Clontech (Palo Alto, CA) and was maintained as monolayer cultures in Dulbecco's modified essential medium supplemented with 10% heat-inactivated fetal bovine serum. Puromycin (Sigma) was added at a final concentration of 3 μg/ml for the selection of pMXpuro-infected cells.

Construction of Plasmids—A retroviral vector derived from a murine leukemia virus, pMXpuro (11), was kindly provided by Prof. T. Kitamura (University of Tokyo, Tokyo, Japan). Open reading frame regions

* This work was supported in part by a grant from the Ministry of Health, Labor, and Welfare (to A. M.). The costs of publication of this article were defrayed in part by the payment of page charges. This article must therefore be hereby marked "*advertisement*" in accordance with 18 U.S.C. Section 1734 solely to indicate this fact.

‡‡ To whom correspondence should be addressed. Tel./Fax: 81-562-44-6595; E-mail: amatsuur@nils.go.jp.

[1] The abbreviations used are: CACT, carnitine-acylcarnitine translocase; CACL, carnitine-acylcarnitine translocase-like; PBS, phosphate-buffered saline; PH, partial hepatectomy; MOPS, 3-morpholinopropanesulfonic acid.

of *mCACT* and *mCACL* were amplified by PCR using EST clones ME624844 and BE372112 as templates, respectively, and cloned into the *Bam*HI-*Bst*XI sites of pMXpuro. For epitope tagging of CACL, a myc-His_6 tag of the pEF4/mycHis vector (Invitrogen Corp.) was inserted immediately before the termination codon of *mCACL* cDNA, and the fusion gene was cloned into the pMXpuro vector.

For the functional expression of *mCACL* in yeast cells, the 1.2-kb *Eco*RI-*Eco*RV fragment of *mCACL* cDNA was inserted into the *Eco*RI-*Pvu*II sites of pKT10 (12). The resultant plasmid, pKT10-mCACL, expressed mCACL driven by promoter of *TDH3*, a gene for glyceraldehyde-3-phosphate dehydrogenase of the budding yeast. The p316CRC1 plasmid was constructed by inserting the yeast gene for CACT (*CRC1*) into the pRS316 vector (13).

For the expression of *mCACL* in *Escherichia coli* cells, the 0.9-kb *Bam*HI-*Xho*I fragment of *mCACL* was isolated from the pMXpuro/mCACL plasmid and inserted into the *Bgl*II-*Sal*I sites of pBAD/gIIIA (Invitrogen Corp.). The resultant plasmid pBAD/CACL-His_6 encoded a CACL-His_6 fusion protein with the pIII signal sequence at the amino terminus, which allowed the recombinant protein to be secreted to plasma membranes. Expression of the fusion protein was induced by the addition of 0.2% arabinose to the LB medium.

Northern Blotting—Total RNA was isolated with TRIzol reagent (Invitrogen Corp.) according to the manufacturer's instructions. Poly(A)$^+$ RNA was isolated from total RNA with a Micro-FastTrack mRNA isolation kit (Invitrogen Corp.) and used for Northern blotting. Poly(A)$^+$ RNA (5 μg) was size-fractionated on a denaturing gel (1.2% agarose, 3.4% formaldehyde, 1× MOPS), transferred to a nylon membrane (Hybond-N, Amersham Biosciences) by capillary transfer, and fixed using standard techniques. A mouse multiple tissue Northern blot (number 7762-1) was purchased from Clontech. After prehybridization, the filters were probed with a 200-bp *CACL* or a 905-bp *CACT* cDNA fragment. An 857-bp β-actin fragment and a 400-bp β_2-microglobulin fragment of mouse were used as controls. The cDNA probes were labeled with [α-^{32}P]dCTP (3000 Ci/mmol; Amersham Biosciences) to a specific activity of >0.5 cpm/μg of DNA using the Megaprime DNA labeling system (Amersham Biosciences).

Antibodies—The following antibodies were purchased: anti-His_6 polyclonal antibody (Medical & Biological Laboratories Co. Ltd., Nagoya, Japan), anti-myc monoclonal antibody (clone 9E10, CRP Inc., Denver, PA), anti-p53 monoclonal antibody (Ab-6, EMD Biosciences, Inc., Darmstadt, Germany), and anti-β-actin monoclonal antibody (clone AC-15, Sigma). Sheep polyclonal antibodies against CACT (14) were gifts from Dr. V. A. Zammit (Hannah Research Institute, Ayr, Scotland, United Kingdom). Anti-mouse CACL polyclonal antibodies were produced as follows. A cDNA fragment corresponding to the carboxyl-terminal 31 amino acids of mouse CACL was inserted into the pGEX-4T-2 vector (Amersham Biosciences). Glutathione *S*-transferase-mCACL fusion protein was produced in *E. coli* DH5α cells and was used as an antigen for immunizing rabbits. The antibodies were affinity purified against an MBP-mCACL fusion protein produced in *E. coli*.

Western Blot Analysis—NIH3T3 cells were washed twice with PBS and suspended in a lysis buffer containing 20 mM Tris-HCl, pH 7.4, 150 mM NaCl, 2 mM EDTA, 1% Nonidet P-40, 1% Na deoxycholate, 0.1% SDS, 50 mM NaF, 1 mM dithiothreitol, 1 mM phenylmethylsulfonyl fluoride, and 1 mM Na_3VO_4. Frozen tissues were disrupted with a Multi-Beads Shocker (Yasui Kikai Co., Osaka, Japan) in 10 volumes of a buffer containing 0.25 M sucrose and 20 mM HEPES, and the homogenate was centrifuged at 600 × *g* for 10 min. The supernatant containing the postnuclear fraction was used as the protein lysate.

The protein lysates were incubated in 2× loading buffer (100 mM Tris-HCl, pH 6.8, 4% SDS, 20% glycerol, and 12% β-mercaptoethanol) at 42 °C for 30 min, separated by SDS-PAGE in a 10% gel, and electroblotted onto polyvinylidene difluoride membranes. To verify the equal loading of proteins in each lane, the blotted membrane was stained with Ponceau-S solution (Sigma). The membranes were blocked in 5% nonfat dry milk in PBS containing 0.1% Tween 20. Immunoblotting was performed with the primary antibodies at dilutions of 1:100 for anti-mCACL, and 1:1000 for anti-CACT and anti-His_6. The incubation with rabbit anti-mCACL antibodies was performed at 4 °C overnight, whereas the incubation with the other antibodies was at room temperature for 1 h. After washing, the membranes were incubated for 60 min with a horseradish peroxidase-conjugated secondary antibody diluted in PBS containing 0.5% nonfat dry milk and 0.1% Tween 20. Blots were developed by enhanced chemiluminescence according to the manufacturer's instructions (ECL Western blotting detection system, Amersham Biosciences).

Immunocytochemistry—Cells were fixed in 4% paraformaldehyde/PBS at room temperature for 10 min and permeabilized with 0.1% Triton X-100 in PBS for 10 min. Cells were then washed in PBS and incubated for 30 min with a blocking solution of 2% normal goat serum in PBS. Coverslips were then incubated for 1 h with the anti-CACL primary antibody diluted at 1:100 in PBS. After three 15-min washes in PBS, cells were incubated with secondary biotinylated anti-rabbit IgG antibody labeled with green fluorescent Alexa Fluor 488 (Molecular Probes Inc., Eugene, OR) at a 1:500 dilution in PBS for 1 h. Cells were washed again with PBS and mounted on glass slides with Vectashield (Vector Laboratories Inc., Burlingame, CA). To stain the mitochondria, 200 nM of a mitochondrion-specific dye (Mitotracker; Molecular Probes Inc.) was incubated with the cells for 30 min before fixation. Slides were examined on a confocal microscope (BX-FLA, Olympus, Tokyo, Japan) equipped for epifluorescence. Montages of images were prepared using PhotoShop 5.0 (Adobe Systems Inc., San Jose, CA).

Complementation of Yeast Mutation—*Saccharomyces cerevisiae* mutants defective in *CIT2* (for peroxisomal citrate synthase) or *CRC1* (for mitochondrial CACT) were obtained from Open Biosystems (Huntsville, AL). A Δ*cit2*::*kanMX* Δ*crc1*::*kanMX* double mutant was constructed by a standard genetic cross. Yeast transformants were selected and grown on minimal medium containing 0.67% yeast nitrogen base without amino acids (YNB-WO, BD Diagnostic Systems, Sparks, MD) supplemented with 0.3% glucose and the appropriate amino acids. Minimal oleate medium contained YNB-WO with amino acids and 0.12% oleate, 0.2% Tween 40 as described previously (15).

Mitochondrial Preparations and Transport Assay—The transport of palmitoyl-[^{14}C]carnitine into mitochondria was measured as described previously (16). Cells grown to confluence on four dishes (15 cm in diameter) were washed twice with PBS and collected by centrifugation at 300 × *g* for 5 min. The cells were resuspended in 2 ml of a homogenization buffer containing 0.25 M sucrose and 20 mM HEPES, pH 7.5, and were homogenized with 20 strokes in a Potter-Elvehjem (Teflon glass) homogenizer. The homogenate was centrifuged at 1,000 × *g* for 7 min. The resultant pellet was homogenized with 2 ml of the buffer and centrifuged again. The postnuclear supernatant was centrifuged at 2,000 × *g* for 30 min to obtain the mitochondrial fraction. The pellet, which contained ~0.2 mg of mitochondria, was resuspended in 250 μl of assay mixture containing 250 mM mannitol, 25 mM HEPES, pH 7.4, 50 μM EDTA, 3 mM ADP, 1 mM maleic acid, 5 mM potassium phosphate, pH 7.4, and palmitoyl-[^{14}C]carnitine (NEC-667, PerkinElmer Life Sciences)-bovine serum albumin complex (at a ratio of 1:3). Protein concentrations were determined using the BCA protein assay kit (Pierce).

Reconstitution of Carnitine-acylcarnitine Translocase in E. coli Cells—The plasmid pBAD/CACL-His_6 or the control vector pBAD/gIIIA was introduced into the *E. coli* strain Rosetta (F^- *ompT* $hsdS_B$ (r_B^- m_B^-) *gal dcm lacY1* pRARE(Cm^R); EMD Biosciences, Inc.). The transformants were grown in LB medium containing 0.2% L-arabinose for 18 h at 30 °C. The cultures were diluted with LB, and the transport reaction was initiated by the addition of palmitoyl-[^{14}C]carnitine (NEC-667, PerkinElmer Life Sciences) to the final concentration of 35 μM. After the reaction at 30 °C, cells were washed twice with PBS, and the incorporation of ^{14}C into the cells was quantified using an LSC-5100 liquid scintillation counter (Aloka, Tokyo, Japan).

Statistical Analysis—Data are expressed as mean ± S.D. The statistical significance of the differences between the control and the experimental group was determined by the unpaired Student's *t* test. Differences were considered significant at $p < 0.05$.

RESULTS

Identification of a Novel Protein Homologous to Carnitine-acylcarnitine Translocase—During a microarray analysis for genes induced after 70% partial hepatectomy (PH) in rats, we found a novel gene whose expression peaked at 6 h after the surgery (data not shown). A mouse clone homologous to the rat gene was obtained from the I.M.A.G.E. consortium, and the sequence analysis of the full-length cDNA identified an open reading frame of 918 nucleotides (Fig. 1*A*). The deduced protein, possessing six membrane-spanning regions (Fig. 1*B*), displayed homology with mitochondrial carrier family proteins. The protein showed the highest similarity (37% identity) with CACT, an inner mitochondrial membrane protein that is essential for the import of long-chain fatty acid moieties into the mitochondrial matrix (6). Thus, we designated the protein as CACL. A data base search using the BLAST program revealed that it is a conserved protein whose homologues are present in human, fly, and worm (Fig. 1*A*). The human orthologue

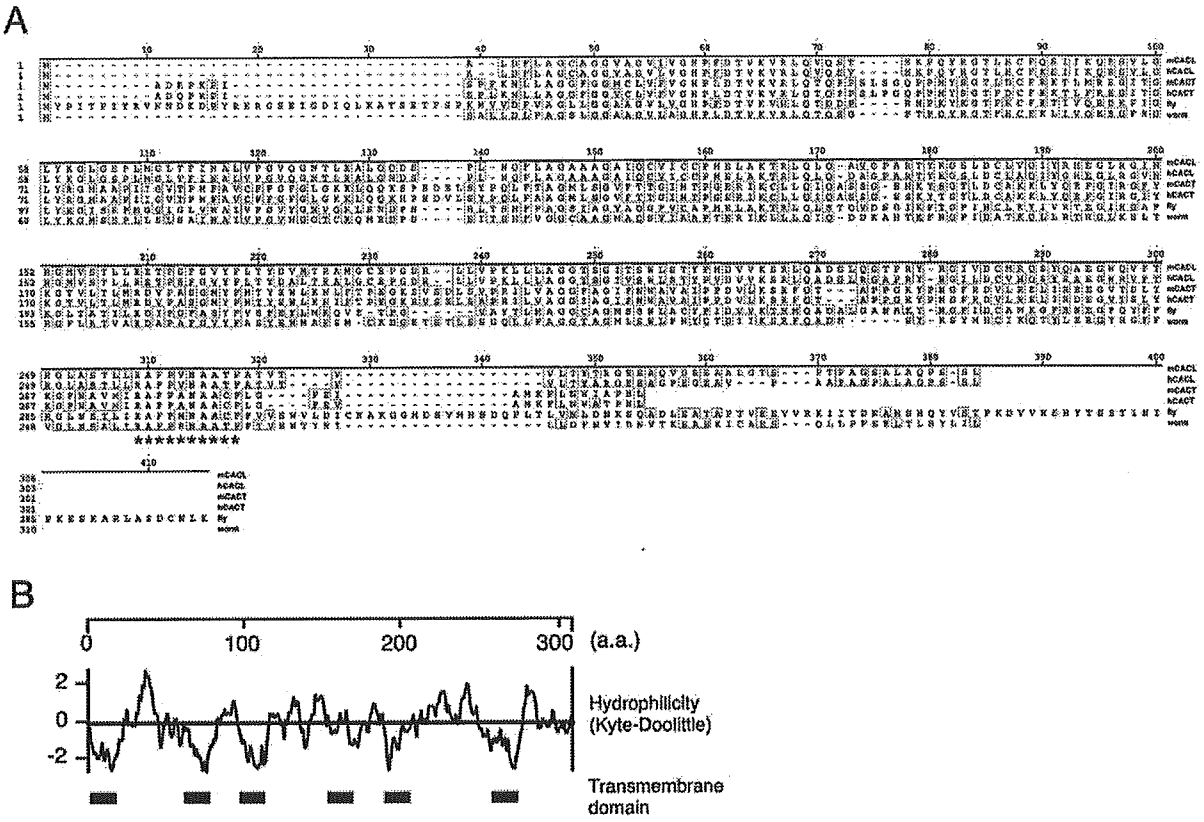

FIG. 1. **A novel CACL in mouse and human.** *A*, sequence alignment of CACLs with CACT. The deduced amino acid sequence of mouse CACL (*mCACL*) shows 37% identity with mouse and human CACT. The human homologue (*hCACL*) is highly conserved (97% identity to mCACL). A data base search identified homologues in *Caenorhabditis elegans* and *Drosophila melanogaster* (C54G10.4 and CG4995, respectively). Amino acid stretches characteristic of carnitine carriers (17) are marked with *asterisks*. *B*, hydrophilicity plot. Hydropathy scores were calculated by the method of Kyte and Doolittle (34). Putative transmembrane regions are shown with *lines*.

(hCACL) has 97% identity with mCACL at the amino acid level and is mapped on chromosome 14q32. A motif within the sixth hydrophobic domain, R(AS)(VF)PANAA(TC)F, has been shown to be conserved within the carnitine carrier subfamily (17). CACL and its homologous proteins all possess the motif, suggesting that they are involved in the transport of acylcarnitine across membranes.

Expression of CACL in Mouse Tissues—The expression pattern in tissues was surveyed using a mouse multiple tissue Northern blot filter. Mouse *CACL* mRNA, ~1.9 kb in length, was expressed in several tissues including heart, brain, liver, and kidney (Fig. 2). This pattern of expression was similar to that of its paralogue *mCACT*, except *CACT* mRNA was rare in brain tissue (Fig. 2*A*). The expression pattern was further confirmed by Western blot analysis using specific antibodies against CACL and CACT. The CACL protein was present at a comparable level in brain, liver, and kidney, whereas CACT expression was barely detectable in brain (Fig. 2*B*). These data suggest that CACL is involved in a biological process similar to that of CACT, but may play a specific role in certain tissues such as brain.

CACL Is Localized to Mitochondria—To determine the subcellular localization of the CACL protein, we constructed NIH3T3 mouse fibroblast cells that stably expressed a CACL fusion protein with a myc-His_6 tag in the carboxyl terminus. Using the anti-myc polyclonal antibody, CACL-myc-His_6 proteins in the fibroblasts were immunostained in a reticulated pattern, which coincided with the mitochondrial staining (Fig. 3, *A–C*). To exclude the possibility that the tag affected the subcellular localization of the protein, we further addressed the localization of CACL using an affinity purified antibody against mCACL. Although we could not detect specific signals of the endogenous protein (data not shown), overexpressed CACL protein without the tag was co-stained with the mitochondrial marker (Fig. 3, *D–F*). Based on these observations, we conclude that CACL, like its homologue CACT, is localized to mitochondria.

CACL Has Palmitoylcarnitine Transporting Activity—In yeast, the transport of acyl units to mitochondria is performed via two pathways, namely the glyoxylate cycle-mediated conversion of acetyl-CoA to succinate that occurs in peroxisomes and the carnitine-dependent acyl-CoA transport. The two pathways have been thought to act in parallel, because disruption of either the *CIT2* gene, which encodes the peroxisomal glyoxylate cycle enzyme citrate synthase, or one of the genes for the carnitine metabolism in mitochondria, did not affect the growth of yeast on oleate, whereas a mutant with both pathways disrupted failed to grow on the plate because of an inability to oxidize the fatty acid (18).

We constructed a double mutant defective in *CIT2* and *CRC1*, the mitochondrial CACT gene in yeast. As reported previously (15), the Δ*crc1* Δ*cit2* mutant could not form colonies on minimal medium containing oleate (Fig. 4*A*), and the defect was rescued by the introduction of the wild-type *CRC1* gene (Fig. 4*B*). Similarly, the heterologous expression of *mCACL* could relieve the growth impairment of the double mutant on

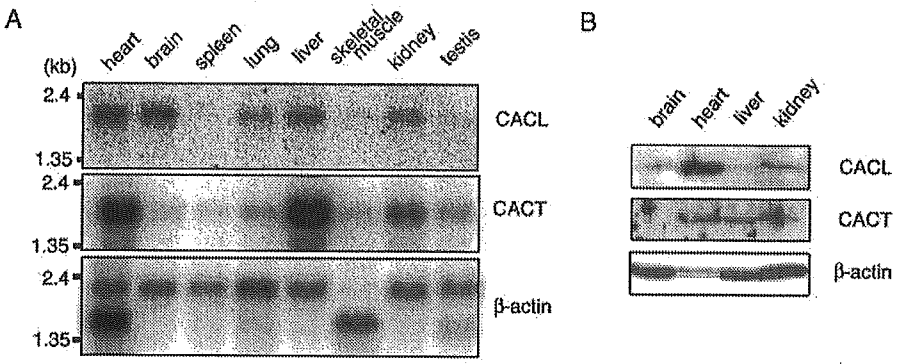

FIG. 2. **Expression of CACL in mouse tissues.** *A*, Northern blot analysis. A multiple tissue Northern blot filter (7762-1, Clontech) was hybridized with a probe corresponding to *mCACL* or *mCACT* cDNA. Each lane contains 2 μg of poly(A)$^+$ RNA. β-Actin cDNA (Clontech) was used as a control probe. Exposure time: 72 h for CACL and 24 h for CACT. *B*, Western blot analysis. An equal amount (100 μg/lane) of the protein lysates from various tissues was separated by SDS-PAGE, followed by Western blot analysis using antibodies against CACL, CACT, and β-actin.

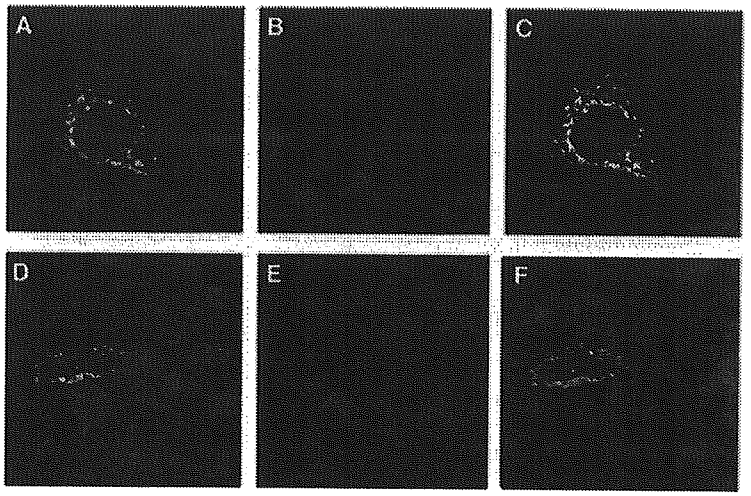

FIG. 3. **CACL is localized to mitochondria.** NIH3T3 cells overexpressing CACL with (*A–C*) or without (*D–F*) the myc-His_6 tag at the carboxyl terminus were fixed and subjected to immunostaining using the anti-His_6 or the anti-CACL antibody. Confocal images of anti-His_6 (*A*) and anti-CACL (*D*) staining (*green*), as well as images of mitochondria staining (*red*; *B* and *E*) with a fluorescent marker Mitotracker (Molecular Probes) are shown. Images were superimposed (*C* and *F*) using PhotoShop 5.0 (Adobe Systems Inc.).

the oleate plate (Fig. 4*C*), suggesting that the CACL protein possesses an enzymatic activity similar to Crc1p.

To examine more directly whether CACL possesses activity similar to that of CACT, we performed a biochemical assay for the acylcarnitine transporting activity of mitochondrial fractions using palmitoyl-[^{14}C]carnitine (16). To this end, we constructed NIH3T3 cells in which *CACL* or *CACT* was overexpressed under the control of the retroviral LTR promoter (Fig. 4*D*). As shown in Fig. 4*E*, liberation of [^{14}C]carnitine, which was produced enzymatically from palmitoyl-[^{14}C]carnitine in the mitochondrial matrix, was observed in the mitochondrial fractions harvested from cells infected with a control vector, and the activity was significantly elevated in cells overexpressing either *CACL* or *CACT*.

Moreover, we constructed a plasmid for the functional expression of the mCACL-His_6 fusion protein in *E. coli*. Cells harboring the plasmid expressed the recombinant protein in an arabinose-dependent manner (Fig. 4*F*), and the expression of mCACL conferred palmitoylcarnitine uptake activity to *E. coli* cells (Fig. 4*G*). Collectively, these data demonstrate that *CACL* indeed encodes a protein with acylcarnitine transporting activity in mitochondria.

Induction of CACL after Partial Hepatectomy and Fasting—As described above, *CACL* was found as a gene whose expression was up-regulated after PH in rats. We addressed whether *CACL* expression was altered in mouse livers after PH.

As shown in Fig. 5*A*, the expression level of the *CACL* transcript in the liver before the operation was low, and was increased at 6–12 h after PH (Fig. 5*A*, *left*). The *CACL* transcript level was slightly increased in sham-operated mice at 6 h (Fig. 5*A*, *right*). Consistently, the amount of the CACL protein was increased at 12 h after PH, whereas the increase was slight after the sham operation (Fig. 5, *B* and *C*). In contrast, a modest increase in *CACT* expression was observed, but its protein level was not increased significantly (Fig. 5, *A–C*). The hepatic surgeries did not affect the protein levels of CACL and CACT in other tissues such as heart (Fig. 5*D*).

Fasting is a stress that is known to cause a metabolic shift to preferentially use free fatty acids. We found that the transcript corresponding to *CACL* was induced markedly in liver after 12 h of fasting (Fig. 6*A*). *CACT* mRNA was also increased under the same condition (Fig. 6*A*). We further examined the amount of CACL protein in several tissues by Western blot analysis using the anti-CACL antibody. As shown in Fig. 6, *B–D*, the protein levels of CACL after fasting were markedly elevated in liver, and increased modestly in heart. In contrast, up-regulation was slight in kidney. We also observed an increase in the amount of CACT in livers and hearts after fasting. These data indicate that the expression of *CACL* and *CACT* is regulated by fasting in a tissue-specific manner and suggest that the induction of these carnitine carriers may contribute to a metabolic change in specific tissues such as the liver.

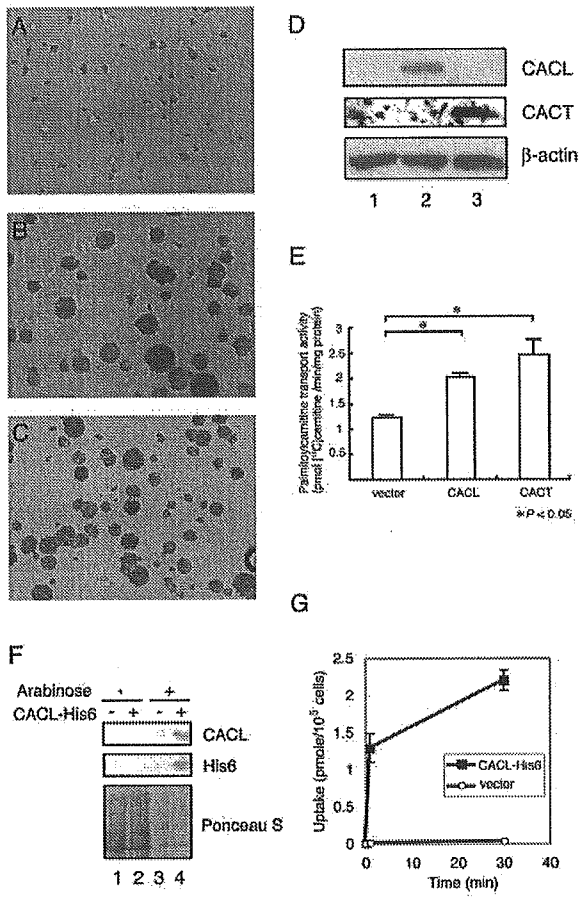

FIG. 4. **CACL possesses acylcarnitine importing activity.** *A–C*, rescue of the growth impairment of the yeast Δ*cit2* Δ*crc1* mutant on oleate by the expression of Crc1p or mCACL. The Δ*cit2* Δ*crc1* cells were transformed with control vector pRS316 (*A*), p316CRC1 (*B*), or pKT10-mCACL (*C*), and the transformants were grown in minimal medium containing 0.3% glucose for 24 h. The cultures were diluted with H_2O and spread onto agar plates of minimal oleate medium. Photographs were taken after incubation for 5 days at 30 °C. *D*, establishment of cells overexpressing *CACL* or *CACT*. NIH3T3 cells were infected with pMXpuro/mCACL (*lane 2*), pMXpuro/mCACT (*lane 3*), or a control vector pMXpuro (*lane 1*), and stable infectants were selected. Cell lysates (100 μg/lane) were analyzed by Western blot analysis using antibodies against mCACL, CACT, and β-actin. *E*, acylcarnitine transport activity in the mitochondrial fraction. Mitochondrial fractions were prepared and used for the acylcarnitine transport assay with palmitoyl-[^{14}C]carnitine (NEC-667, PerkinElmer Life Sciences) as described under "Experimental Procedures." The data presented are average ± S.D. of three independent experiments. *F–G*, functional expression of mCACL in *E. coli*. *E. coli* cells possessing pBAD/CACL-His_6 (*lanes 2* and *4*) or a control vector pBAD/gIIIA (*lanes 1* and *3*) were grown in the presence (*lanes 3* and *4*) or absence (*lanes 1* and *2*) of 0.2% arabinose for 18 h at 30 °C. Lysates were subjected to Western blot analysis using anti-CACL or anti-His_6 antibodies (*F*). In *G*, *E. coli* cells grown in LB + 0.2% arabinose were incubated with palmitoyl-[^{14}C]carnitine, and the incorporation of ^{14}C into cells at 30 °C was measured as described under "Experimental Procedures." The data presented are average ± S.D. of three independent experiments.

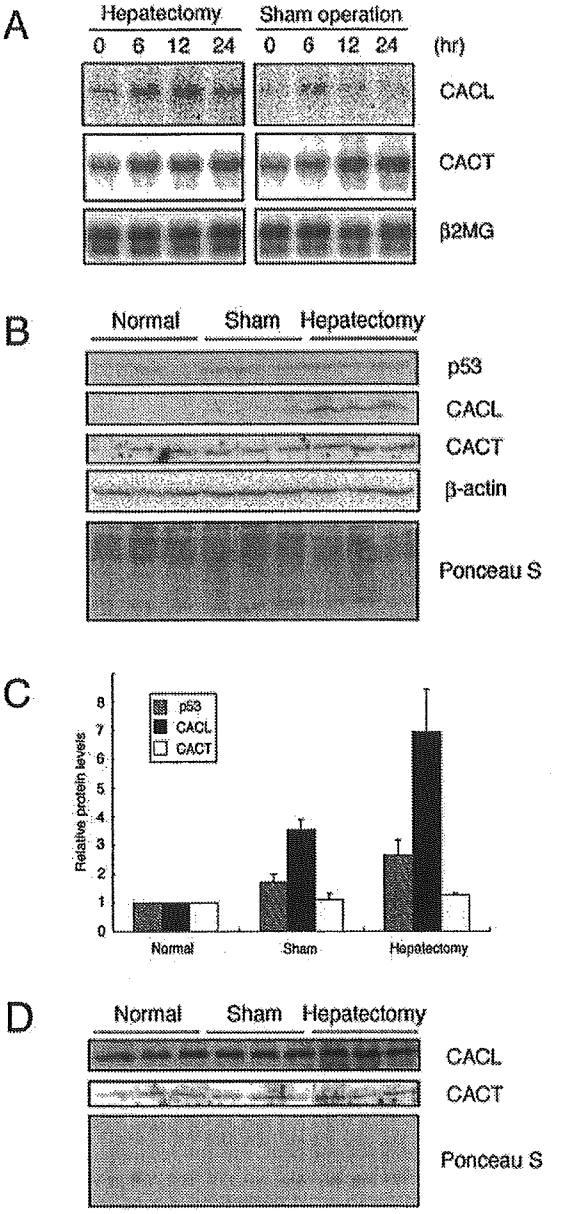

FIG. 5. **Induction of CACL after partial hepatectomy.** *A*, Northern blot analysis. A 70% hepatectomy was performed at time 0, and the remnant regenerating livers were collected at the indicated times after surgery. Livers were also collected from sham-operated C57BL/6 mice. Poly(A)$^+$ RNAs (5 μg/lane) were subjected to Northern blot analysis with *mCACL*, *mCACT*, and β_2-microglobulin cDNA probes. *B* and *C*, Western blot analysis of liver lysates. Livers were collected from three mice without operations and from mice 12 h after the hepatectomy or a sham operation. Postnuclear lysates were subjected to Western blot analysis using antibodies against p53, mCACL, CACT, and β-actin. In *C*, protein levels were quantitatively measured, and normalized -fold induction after the operations was calculated. Values shown are average ± S.D. for three different mice. Note that the protein levels of p53 increased after the partial hepatectomy, as reported previously (35). *D*, Western blot analysis of heart lysates. Hearts were collected at the same time points as in *B*, and postnuclear lysates were subjected to Western blot analysis.

DISCUSSION

In the present study we identified CACL, a novel mammalian protein that is localized to mitochondria and exhibits acylcarnitine transporting activity. The *CACL* transcript was found in tissues such as heart and liver, where its homologue *CACT* was expressed at a high level. In humans, patients with a CACT deficiency exhibited various cardiac symptoms and abnormal liver functions (7–9). Thus, CACL may not be able to compensate for CACT function in fatty acid metabolism of these tissues.

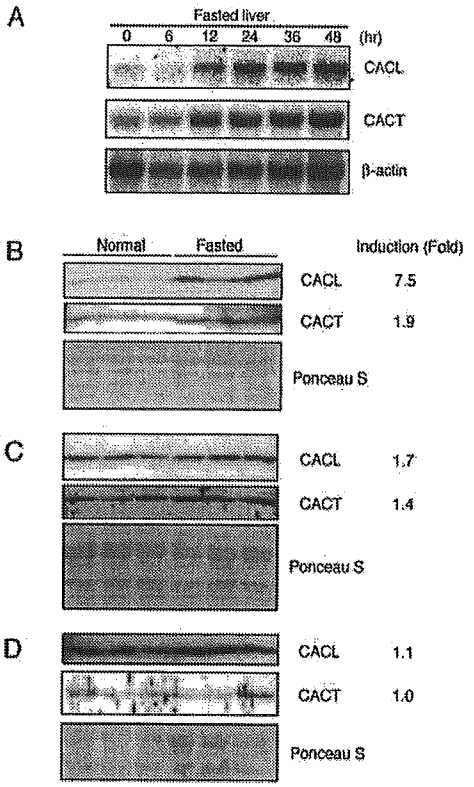

FIG. 6. **Induction of CACL after fasting.** *A*, Northern blot analysis. Mice that fasted for the indicated times were sacrificed, and poly(A)$^+$ RNAs were collected from the livers. Northern blot analysis was performed with probes for *mCACL* mRNA, *mCACT* mRNA, and β-actin mRNA. Each lane contained 10 μg of poly(A)$^+$ RNA. *B–D*, Western blot analysis. Protein lysates were prepared from the tissues of three mice before or after a 48-h fast. Western blot analysis was performed using antibodies against CACL and CACT. Each lane contained 100 μg of protein. Protein levels were quantitatively measured, and normalized -fold induction after fasting was calculated. Values shown are average for three different mice. Tissues examined were as follows: *B*, liver; *C*, heart; and *D*, kidney.

In contrast, the brain is a unique organ in which *CACL* is expressed at higher levels than is *CACT*. Although peroxisomal β-oxidation enzymes are expressed in brain (19), there have been no reports to show that the mitochondrial β-oxidation pathway is operating in the brain. The presence of the *CACL* transcript suggests that acylcarnitine might be used in this organ. The brain contains relatively high amounts of long-chain polyunsaturated fatty acids, such as docosahexaenoic acid, which are critical for its functions (20). It was recently reported that a novel carnitine palmitoyltransferase was expressed specifically in brain and testis (21) and that carnitine transporters on the plasma membrane, which are involved in carnitine uptake, were expressed in brain (22). Together with the carnitine-handling enzymes expressed in brain, CACL might have specialized roles in the metabolism of a distinct class of fatty acids that are involved in brain function.

The liver is a unique organ with a regenerative capacity. After 70% of the mass is surgically removed, the residual hepatic lobes enlarge to restore the original mass within 7 days, and vascularization is completed within the subsequent 7 days (23). A variety of genes are involved in the whole process of liver regeneration, although the molecular mechanisms underlying the process remain unknown. Recently, Su *et al.* (24) reported a microarray-based study of the gene expression profile during the priming phase of liver regeneration in mice. They reported up-regulation of phosphoenolpyruvate carboxykinase and glucose 6-phosphatase, which are involved in maintaining glucose levels after an acute loss of liver mass. Thus, a subtle regulation that switches energy metabolism appears to occur in the regenerating liver.

Carnitine has been thought to be one of the key factors in the regulation of liver regeneration, because the carnitine content in the liver increases after PH (25) and liver regeneration is accelerated by the administration of carnitine to hepatectomized rats (26). In addition, increases in the mRNA levels of carnitine palmitoyltransferase I and II have been observed in regenerating livers (27). Taken together, these results suggest that the carnitine-dependent pathway is important for energy supply when the liver, a major organ critical to maintaining metabolic and biosynthetic homeostasis, is partially removed. In agreement with this notion, we found that the level of CACL protein was elevated after PH. This acylcarnitine carrier may be involved in one of the key steps that regulate cellular metabolism during liver regeneration.

A change in the energy source from glucose to free fatty acids has been widely observed as an adaptive response to fasting (28). In the fasting heart, intracellular droplet accumulation was observed (29), and the content of glycerides and glycogen was increased through the inhibition of the glycolytic pathway and the enhancement of the β-oxidation pathway (30). A recent study using oligonucleotide microarrays revealed that the expression of a wide range of cardiac genes was affected by fasting, including the up-regulation of genes for fatty acid oxidation and gluconeogenesis and the down-regulation of genes for glycolysis (31). We found that *CACL* and *CACT* were up-regulated at the mRNA level in liver, and furthermore, fasting increased the amount of the CACL and CACT proteins in heart and liver. These two organs are prominent in the use of fatty acids upon starvation; fasted cardiac muscles directly use fatty acids as an energy source, whereas hepatic metabolism of fatty acids is mostly directed toward the synthesis of ketone bodies for use as energy sources in tissues such as brain (32). Thus, the up-regulation of CACL and CACT may contribute to the adaptation of the whole body to fasting.

Systemic energy metabolism has been shown to be tightly regulated by the action of hormones, and a disruption of this coordinated regulation causes disorders such as obesity and diabetes (33). Further studies of the coordinating mechanisms of glucose and lipid metabolism in the responsible organs will provide insights for the development of novel approaches to therapy or prevention of these disorders.

Acknowledgments—We thank Dr. Yoshiyuki Takahara (Ajinomoto Co., Inc.) for providing the microarray data, Dr. Toshio Kitamura for plasmids, Dr. V. A. Zammit for antibodies, and Dr. Satoshi Kametaka (Osaka University) for technical advice. We are grateful to Eiji Hayashi, Makoto Kimura, and Yayoi Tanaka (National Institute for Longevity Sciences) for technical assistance and to members of the Department of Geriatric Research for helpful discussions.

REFERENCES

1. Wallis, J. G., Watts, J. L., and Browse, J. (2002) *Trends Biochem. Biosci.* **27,** 467–473
2. Hale, D. E., and Bennett, M. J. (1992) *J. Pediatr.* **121,** 1–11
3. Pande, S. V. (1975) *Proc. Natl. Acad. Sci. U. S. A.* **72,** 883–887
4. Ramsay, R. R., Gandour, R. D., and van der Leij, F. R. (2001) *Biochim. Biophys. Acta* **1546,** 21–43
5. Indiveri, C., Iacobazzi, V., Giangregorio, N., and Palmieri, F. (1997) *Biochem. J.* **321,** 713–719
6. Huizing, M., Iacobazzi, V., Ijlst, L., Savelkoul, P., Ruitenbeek, W., van den Heuvel, L., Indiveri, C., Smeitink, J., Trijbels, F., Wanders, R., and Palmieri, F. (1997) *Am. J. Hum. Genet.* **61,** 1239–1245
7. Stanley, C. A., Hale, D. E., Berry, G. T., Deleeuw, S., Boxer, J., and Bonnefont, J. P. (1992) *N. Engl. J. Med.* **327,** 19–23
8. Pande, S. V., Brivet, M., Slama, A., Demaugre, F., Aufrant, C., and Saudubray, J. M. (1993) *J. Clin. Invest.* **91,** 1247–1252
9. Pande, S. V. (1999) *Am. J. Med. Sci.* **318,** 22–27

10. Higgins, G. M., and Anderson, R. M. (1931) *Arch. Pathol.* **12,** 186–202
11. Onishi, M., Kinoshita, S., Morikawa, Y., Shibuya, A., Phillips, J., Lanier, L. L., Gorman, D. M., Nolan, G. P., Miyajima, A., and Kitamura, T. (1996) *Exp. Hematol.* **24,** 324–329
12. Tanaka, K., Nakafuku, M., Tamanoi, F., Kaziro, Y., Matsumoto, K., and Toh-e, A. (1990) *Mol. Cell. Biol.* **10,** 4303–4313
13. Sikorski, R. S., and Hieter, P. (1989) *Genetics* **122,** 19–27
14. Fraser, F., and Zammit, V. A. (1999) *FEBS Lett.* **445,** 41–44
15. van Roermund, C. W. T., Hettema, E. H., van den Berg, M., Tabak, H. F., and Wanders, R. J. A. (1999) *EMBO J.* **18,** 5843–5852
16. Murthy, M. S., and Pande, S. V. (1984) *J. Biol. Chem.* **259,** 9082–9089
17. De Lucas, J. R., Dominguez, A. I., Valenciano, S., Turner, G., and Laborda, F. (1999) *Arch. Microbiol.* **171,** 386–396
18. van Roermund, C. W. T., Elgersma, Y., Singh, N., Wanders, R. J. A., and Tabak, H. F. (1995) *EMBO J.* **14,** 3480–3486
19. Knoll, A., Sargueil, F., Salles, J., Cassagne, C., and Garbay, B. (1999) *Brain Res. Mol. Brain Res.* **74,** 217–220
20. Uauy, R., Hoffman, D. R., Peirano, P., Birch, D. G., and Birch, E. E. (2001) *Lipids* **36,** 885–895
21. Price, N. T., van der Leij, F. R., Jackson, V. N., Corstorphine, C. G., Thomson, R., Sorensen, A., and Zammit, V. A. (2002) *Genomics* **80,** 433–442
22. Eraly, S., and Nigam, S. (2002) *Biochem. Biophys. Res. Commun.* **297,** 1159–1166
23. Michalopoulos, G. K., and DeFrances, M. C. (1997) *Science* **276,** 60–66
24. Su, A. I., Guidotti, L. G., Pezacki, J. P., Chisari, F. V., and Schultz, P. G. (2002) *Proc. Natl. Acad. Sci. U. S. A.* **99,** 11181–11186
25. Lai, H. S., Chen, Y., and Chen, W. J. (1998) *World J. Surg.* **22,** 42–46; 46–47
26. Holecek, M., Simek, J., Zadak, Z., and Blaha, V. (1989) *Physiol. Bohemoslov* **38,** 503–508
27. Asins, G., Rosa, J. L., Serra, D., Gil-Gomez, G., Ayte, J., Bartrons, R., Tauler, A., and Hegardt, F. G. (1994) *Biochem. J.* **299,** 65–69
28. Neely, J. R., and Morgan, H. E. (1974) *Annu. Rev. Physiol.* **36,** 413–459
29. Adams, M. G., Barer, R., Joseph, S., and Om'Iniabohs, F. (1981) *J. Pathol.* **135,** 111–126
30. Denton, R. M., and Randle, P. J. (1967) *Biochem. J.* **104,** 416–422
31. Suzuki, J., Shen, W. J., Nelson, B. D., Selwood, S. P., Murphy, G. M., Jr., Kanefara, H., Takahashi, S., Oida, K., Miyamori, I., and Kraemer, F. B. (2002) *Am. J. Physiol.* **283,** E94–E102
32. Mitchell, G. A., Kassovska-Bratinova, S., Boukaftane, Y., Robert, M. F., Wang, S. P., Ashmarina, L., Lambert, M., Lapierre, P., and Potier, E. (1995) *Clin. Invest. Med.* **18,** 193–216
33. Saltiel, A. R., and Kahn, C. R. (2001) *Nature* **414,** 799–806
34. Kyte, J., and Doolittle, R. F. (1982) *J. Mol. Biol.* **157,** 105–132
35. Inoue, Y., Tomiya, T., Yanase, M., Arai, M., Ikeda, H., Tejima, K., Ogata, I., Kimura, S., Omata, M., and Fujiwara, K. (2002) *Hepatology* **36,** 336–344

Identification of a Large Novel Imprinted Gene Cluster on Mouse Proximal Chromosome 6

Ryuichi Ono,[1,2,3] Hirosuke Shiura,[1] Hiroyuki Aburatani,[4] Takashi Kohda,[1,3] Tomoko Kaneko-Ishino,[3,5] and Fumitoshi Ishino[1,3,6]

[1]*Gene Research Center, Tokyo Institute of Technology, Yokohama 226-8501, Japan;* [2]*Research Fellow of the Japan Society for the Promotion of Science, Tokyo 102-8471, Japan;* [3]*CREST, Japan Science and Technology Corporation (JST), Saitama 332-0012, Japan;* [4]*Genome Science Division, Research Center for Advanced Science and Technology, The University of Tokyo, Tokyo 153-8904, Japan;* [5]*Tokai University, School of Health Sciences, Kanagawa 259-1193, Japan*

Mice with maternal duplication of proximal chromosome 6 die in utero at an early embryonic stage. Recently, two imprinted genes, paternally expressed *Sgce* and maternally expressed *Asb4*, were identified in this region. This report analyzes the imprinting status of genes within a 1-Mb region containing these two genes. *Peg10*, which is next to *Sgce*, shows complete paternal expression, like *Sgce*. Conversely, *Neurabin*, *Pon2*, and *Pon3* show preferential maternal expression at embryonic stages, although they all show biallelic expression in neonatal tissues. These results demonstrate that there is a large novel imprinted gene cluster in this region. 5′-RACE (Rapid Amplification of cDNA Ends) analysis of *Peg10* revealed the existence of a novel first exon separate from the second exon, which encoded two putative ORFs similar to the viral Gag and Pol proteins. A differentially methylated region established in sperm and eggs is located just within the region containing the two first exons of *Peg10* and *Sgce*, and may play an important role in regulating the two paternally expressed genes: *Peg10* and *Sgce*.

[Supplemental material is available online at www.genome.org. The sequence data from this study have been submitted to DDBJ under accession nos. AB091827–AB091829.]

Maternal uniparental duplication in mouse proximal chromosome 6 causes early embryonic lethality (Beechey 2000; also see http://www.mgu.har.mrc.ac.uk/imprinting/imprinting.html). Previously, we identified *Peg1/Mest* as the first imprinted gene in the mouse proximal chromosome 6 (Kaneko-Ishino et al. 1995). However, *Peg1/Mest*-deficient mice show perinatal growth retardation and abnormal maternal behavior, but do not show early embryonic lethality (Lefebvre et al. 1998). Recently, the existence of two imprinted regions has been demonstrated in this region; mice with a maternal duplication proximal to T77H die in utero before 11.5 dpc, whereas those with a duplication distal to T77H show growth retardation (Beechey 2000). *Peg1/Mest* maps to the latter region, and two novel imprinted genes, paternally expressed *Sgce* and maternally expressed *Asb4*, have been identified in the former region (Piras et al. 2000; Mizuno et al. 2002). We have also reported that human retrotransposon-derived *PEG10*, which is adjacent to *SGCE*, is a paternally expressed imprinted gene (Ono et al. 2001).

Because many imprinted genes form clusters in some chromosome regions, it is very possible that there is a large imprinted gene cluster in the *Sgce-Asb4* region. Therefore, we analyzed the imprinting status of six other genes in this region (*Cas1*, *Peg10*, *Neurabin*, *Pon1*, *Pon3*, and *Pon2*) and showed that four genes were imprinted. *Peg10* was paternally expressed, whereas the other three genes showed preferential maternal expression in the embryonic stage. In relation to these imprinted genes, we discuss the phenotypes observed in mice with maternal duplication of proximal chromosome 6 (early embryonic lethality and perinatal growth retardation) and in human maternal disomy of chromosome 7, which is associated with the growth retardation phenotype known as Silver-Russell syndrome (SRS; OMIM No.180860).

[6]Corresponding author.
E-MAIL fishino@bio.titech.ac.jp; FAX 81-45-924-5814.
Article and publication are at http://www.genome.org/cgi/doi/10.1101/gr.906803.

RESULTS

Gene Alignment and Analysis of CpG Islands of the *Col1a2–Asb4* Region in the Mouse

Nine genes in mouse proximal chromosome 6 map to a 1-Mb region between 1.2 and 2.2 Mb of the *Mus musculus* Whole-Genome Shotgun (WGS) supercontig Mm6_WIFeb01_97 (GenBank accession no. NW_000272): *Col1a2*, *Cas1*, *Sgce*, *Peg10*, *Neurabin*, *Pon1*, *Pon3*, *Pon2*, and *Asb4* (from proximal to distal, Fig. 1A). This gene alignment is conserved in the human syntenic 7q21 region (data not shown). In this report, we characterize the imprinting status of six of these genes (*Cas1*, *Peg10*, *Neurabin*, *Pon1*, *Pon3*, and *Pon2*), because *Sgce* and *Asb4* are already known to be imprinted and *Col1a2* is reported to show biallelic expression (Piras et al. 2000; Mizuno et al. 2002). This region contained four CpG islands (CGIs) corresponding to the promoter regions of the *Cas1*, *Peg10-Sgce*, *Neurabin*, and *Pon2* genes. Bisulfite sequencing analyses of both day 10 embryo and placenta showed that three regions were nonmethylated (Fig. 1B), and that of *Peg10-Sgce* was differentially methylated (Fig. 2A).

We previously reported that human *PEG10* was derived from a Sushi-ichi retrotransposon encoding two ORFs (ORF1 and ORF2) showing similarity to retroviral Gag and Pol proteins, respectively (Fig. 2A; Poulter and Butler 1998; Ono et al. 2001). *Peg10* exists in all five mammals that we have exam-

13:1696–1705 ©2003 by Cold Spring Harbor Laboratory Press ISSN 1088-9051/03 $5.00; www.genome.org

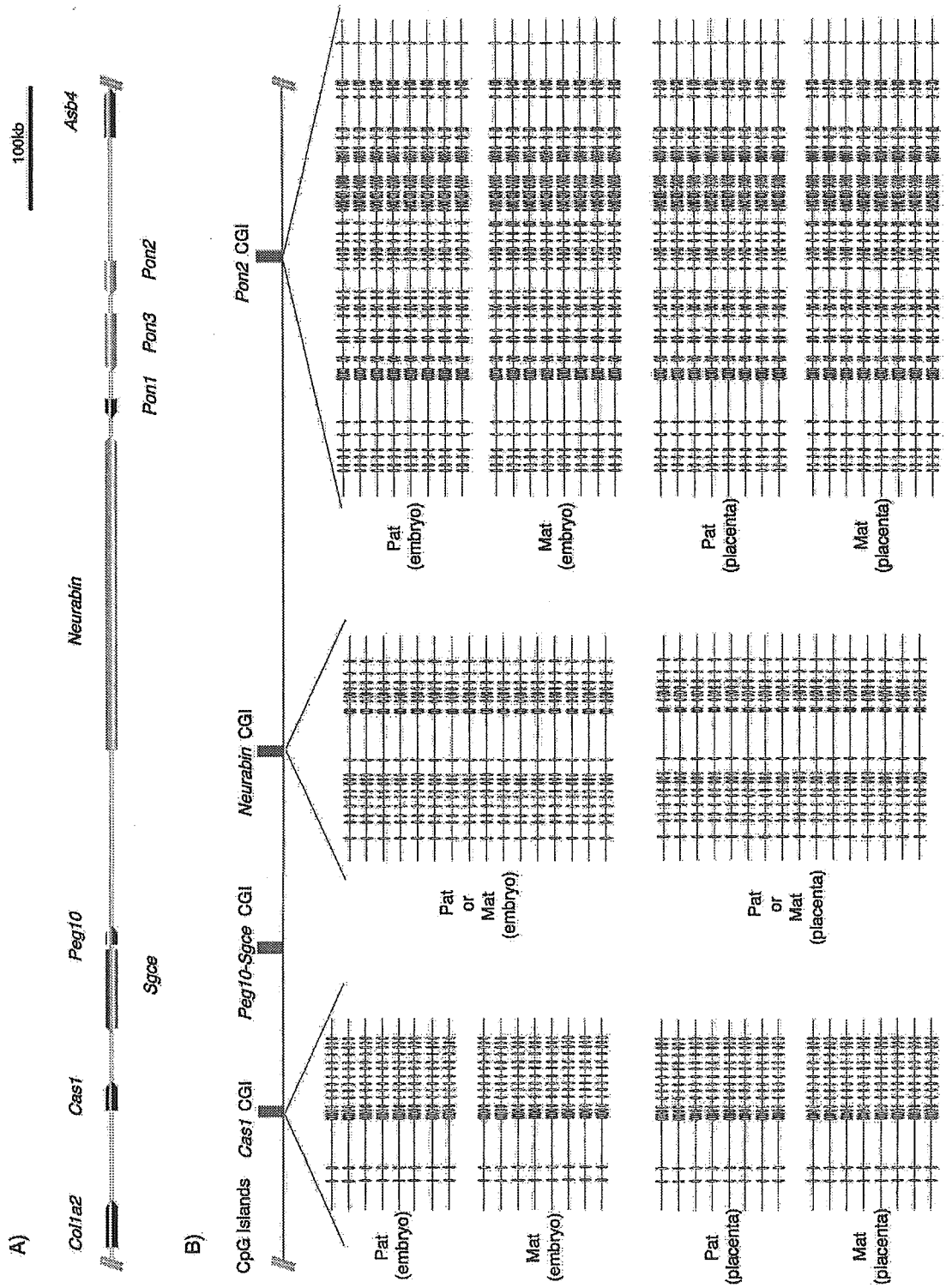

Figure 1 (Legend on next page)

ined (human, cat, dog, olive baboon, and chimpanzee), in the same location as in the mouse (Fig. 1A; GenBank accession no. AC069292, AC108197, AC113572, AC092529, and AC094111, respectively). Expressed sequence tags (ESTs) corresponding to *Peg10* are also registered for the cow, rat, mink, and pig (GenBank accession no. AV608102, AI599367, MVU00594, and BF191703, respectively). Therefore, retrotransposon-derived *Peg10* is highly conserved in mammals.

Genomic Structure and Verification of Imprinting of Mouse *Peg10*

We determined the full-length sequence of *Peg10*, which consists of 6407 bp, by 5′-RACE (Rapid Amplification of cDNA Ends; GenBank accession no. AB091827). The first exon of *Peg10* was identified 6.5 kb upstream of the second exon and was within 250 bp of the first exon of *Sgce*, which is oriented in a head-to-head manner (Fig. 2A). The genomic structure of these two genes is also conserved in the human genome (data not shown). Therefore, it is not an intron-less gene, as we previously reported in humans (Ono et al. 2001).

A CGI overlaps the first two exons of *Sgce* and *Peg10* (Fig. 2A), and there are 12 direct repeats of a 29-bp GC-rich sequence in the *Peg10* intron 1, just downstream of the first *Peg10* exon (Fig. 2B). Bisulfite sequencing analyses showed that the whole CGI was differentially methylated in paternal and maternal alleles in both day 10 embryo (Fig. 2A, lower part) and placenta (data not shown). Furthermore, it was revealed that differential methylation was already established in oocytes and sperm. Therefore, this region is the primary differentially methylated region (DMR), which indicates that it has an important function in regulating the paternal expression of both *Peg10* and *Sgce* (see following).

To verify tissue-specific expression, we carried out Northern blot analyses using a *Peg10* 3′untranslated region (UTR) fragment as a probe. As shown in Figure 2C, a high level of *Peg10* expression was observed only in placentas. The major transcript was estimated to be ~6.5 kb, which is consistent with the full-length cDNA that we identified. Strong expression of human *SGCE* and *PEG10* in placenta has been reported previously (McNally et al. 1998; Ono et al. 2001).

To verify the imprinting status of *Peg10*, we examined DNA polymorphisms in the *Peg10* 3′UTR between JF1 and C57BL/6 (the G and A residues indicated by arrows in Fig. 2D, respectively) by direct sequencing. In day 10 F_1 embryos of the crosses (B6 × JF1 and JF1 × B6), only paternal G residues were detected in the placentas, yolk sacs, and neonatal brains in the former, and only paternal A residues were detected in the latter samples. Therefore, paternal expression of *Peg10* was confirmed in mice, as occurs with human *PEG10*.

Genes Showing Preferential Maternal Expression

To test the imprinting status of the remaining five genes (*Cas1*, *Neurabin*, *Pon1*, *Pon3*, and *Pon2*), we examined DNA polymorphisms between JF1 and C57BL/6. Allele-specific expression analyses were carried out using a restriction fragment length polymorphism (RFLP) method combined with the Hot-stop RT-PCR method (Uejima et al. 2000). To exclude the possible misinterpretation of imprinting status because of the existence of overlapping RNAs, we confirmed that no other cDNA bands of different sizes or genomic DNA bands of the same size were detected in RT-PCR experiments for each gene, when the two primers were located in different exons. In addition, the amplified bands were directly sequenced to confirm that they were derived from the genes in question.

Cas1, which encodes a putative glycosyltransferase, is a conserved gene found in humans, *Drosophila*, plants, and bacteria (Janbon et al. 2001). In the mouse, RT-PCR experiments with RNA from a range of adult tissues showed that *Cas1* was expressed ubiquitously (Fig. 3A). In the RFLP analysis, *Cas1* showed complete or equal biallelic expression in neonatal brain. It was also biallelically expressed in day 10 and 13 embryo, placenta, and yolk sac samples, but there seemed to be weak maternal biases, especially in extraembryonic tissues (data not shown). Therefore, an RFLP analysis combined with Hot-stop PCR was performed to quantify the expression of each allele precisely. The levels of JF1 and B6 expression went up and down reciprocally in two reciprocal F_1 samples (Fig. 3B), indicating its imprinting. However, the expression ratios of maternal/paternal alleles (M/P values) in these samples were small (no more than twofold) and were not conclusive.

Neurabin was first isolated as an actin filament (F-actin)-binding protein in the rat. It regulates synapse formation in vitro and is specifically expressed in neural tissues (Nakanishi et al. 1997). As shown in Figure 3C, *Neurabin* was strongly expressed in the brain. Allelic expression analysis using RFLP with Hot-stop PCR showed biallelic expression of *Neurabin* in the neonatal brain, and preferential maternal expression was observed in placenta (day 10) and yolk sac (day 10 and 13) samples (Fig. 3D). In these tissues, the ratio of expression of a 240-bp band derived from the B6 allele to that of a 100-bp band from the JF1 allele was constantly higher in (B6 × JF1) F_1 samples and lower in reciprocal (JF1 × B6) F_1 samples. The M/P values of placentas were 3.5 and 2.6 (day 10) in (B6 × JF1) F_1 and (JF1 × B6) F_1, respectively, and these values for yolk sac samples were 2.2 and 4.9 (day 10) and 2.0 and 4.6 (day 13). Because it is apparent that placenta samples from day 13 contain significant amounts of maternal tissue, we did not analyze these samples. We also cannot exclude the possibility of maternal tissue contamination from placenta samples completely, even when isolated from day 10 conceptus, whereas yolk sac samples can be recovered free from maternal contamination. Therefore, we conclude that *Neurabin* is

Figure 1 Genomic structure of the *Col1a2-Asb4* region in the mouse. (*A*) Physical map of the genes identified in a 1-Mb region in the *Mus musculus* WGS supercontig Mm6_WIFeb01_97 (GenBank accession no. NW_000272). The arrows show the direction of each transcription unit, and imprinted genes are indicated by color: red and pink indicate strong and weak preferential maternal expression, respectively, and blue indicates complete paternal expression. Genes showing no expression biases between parental alleles are shown in black. (*B*) CpG islands (CGIs) and their DNA methylation states in the domain. There are four CGIs (length over 300 bp) shown in green boxes in the *Col1a2-Asb4* region, and the three nonmethylated CGIs determined by bisulfite sequencing of genomic DNA isolated from (B6 × JF1) F_1 embryo and placenta (day 10) are shown. DNA polymorphisms were used to determine paternal and maternal alleles of *Cas1* CGI and *Pon2* CGI, and showed that both alleles were nonmethylated in this region: No available DNA polymorphisms were found in *Neurabin* CGI, but no methylated CpGs were observed in this region either. Each horizontal line indicates the sequence from a single clone. Each CpG dinucleotide is represented by an oval. White and black ovals indicate nonmethylated and methylated CpGs, respectively. Details of the differentially methylated region of the *Peg10-Sgce* CGI are shown in Fig. 2A.

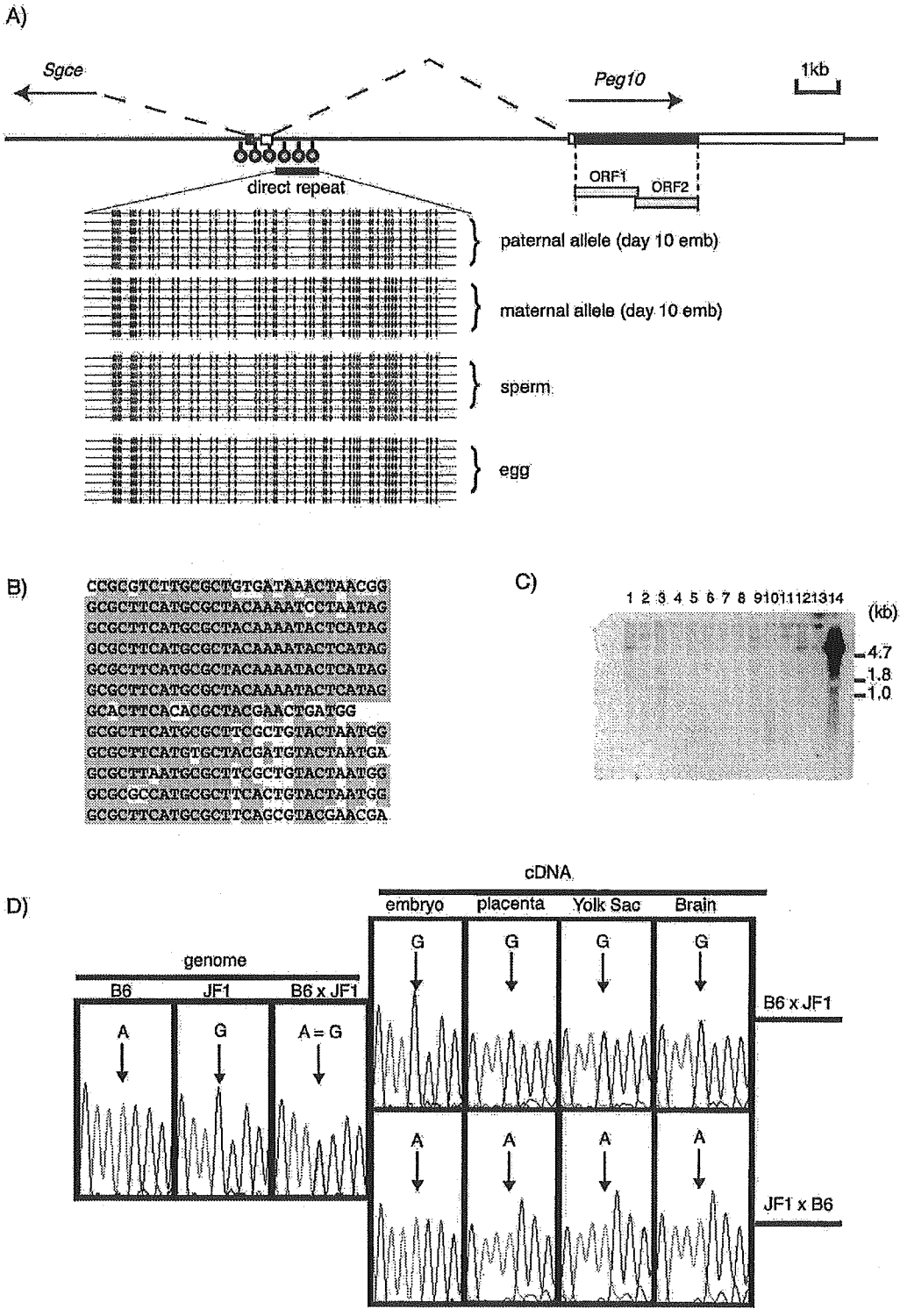

Figure 2 (Legend on next page)